Alma Mater Studiorum · Università di Bologna

SCUOLA DI SCIENZE
Corso di Laurea Magistrale in Matematica

A MATHEMATICAL MODEL OF THE MOTOR CORTEX

Tesi di laurea in Analisi Matematica

Relatore:
Chiar.ma Prof.ssa
Giovanna Citti

Correlatore:
Chiar.mo Dott.
Emre Baspinar

Presentata da:
Caterina Mazzetti

II Sessione
Anno Accademico 2016/2017

Alla mamma, al babbo, a Michele
e a Tu-Sai-Chi

Abstract

In this work we present a geometric model of motor cortex that generalizes an already existing model of visual cortex. The thesis opens by recalling the notions of fiber bundles, principal bundles, Lie groups, sub-Riemannian geometry and horizontal tangent bundle. In particular, we enunciate Chow's Theorem which ensures that if the generators of the horizontal tangent bundle satisfy the Hörmander condition, any couple of points can be connected by integral curves of the generators. Then we recall the model of the visual cortex proposed by Citti-Sarti, which describes the set of simple cells as a Lie group with sub-Riemannian metric.
The original part of the thesis is the extension to the motor cortex. Based on neural data, collected by Georgopoulos, we study the set of motor cortical cells and we describe them as a principal bundle. The fiber contains the movement direction and shapes the hypercolumnar structure measured. Finally we determine the intrinsic coordinates of the motor cortex, studying the cellular response to the motor impulse.

Sommario

In questa elaborato presentiamo un modello geometrico di corteccia motoria che generalizza un precedente modello di corteccia visiva. La tesi si apre richiamando le nozioni principali di fibrati tangenti, fibrati principali, gruppi di Lie e di geometria sub-Riemanniana e fibrato tangente orizzontale. In particolare, enunciamo il Teorema di Chow che assicura che se i generatori del fibrato tangente orizzontale soddisfano la condizione di Hörmander, allora ogni coppia di punti può essere connessa da curve integrali dei generatori. Richiamiamo poi il modello di corteccia visiva proposto da Citti-Sarti che descrive l'insieme delle cellule semplici come un gruppo di Lie con metrica sub-Riemanniana.
La parte originale della tesi consiste nell' estensione alla corteccia motoria. Basandoci sui dati neurofisiologici raccolti da Georgopoulos, studiamo l'insieme delle cellule motorie e ne modelliamo la struttura tramite un fibrato principale. La fibra contiene la direzione del movimento a da' luogo alla struttura ipercolonnare misurata. Infine, determiniamo le coordinate intrinseche della corteccia motoria studiandone la risposta cellulare ad un impulso motorio.

Introduction

In this thesis we propose a model of the motor cortex, inspired to previous models of the visual cortex.
The primary visual cortex has been described as a fiber bundle by Petitot and Tondut [22], [23] and as a Lie group with sub-Riemannian metric by Citti-Sarti [6]. The elements which allow to describe the functional architecture of the visual cortex are:

- cells selectivity properties of geometric features. In particular, the position and orientation selection by means of the simple cells. This means that simple cells response is maximal when a certain visual input occurs in a precise position and orientation.

- The hypercolumnar structure. For simple cells (sensitive to orientation) columnar structure means that to every retinal position is associated a set of cells (hypercolumn) sensitive to all the possible orientations. This structure is described as a principal bundle, more precisely as a fiber bundle with retinal base $\mathbb{R}^2$ and fiber S^1. The total space of the fiber bundle is therefore $\mathbb{R}^2 \times S^1$. Note that cortex is a surface, hence a 2D structure, in which the hypercolumns are implemented by a process of dimensional reduction that gives rise to orientation maps, called pinwheels. Furthermore, simple cells activity provides the cortical space $\mathbb{R}^2 \times S^1$ with a Lie group structure with sub-Riemannian metric.

A sub-Riemannian manifold is a triple (M, Δ, g), where M is a Riemannian manifold of dimension n, Δ is a distribution subset of the tangent bundle and g is a scalar product defined on Δ (see [20] for a general presentation). If $X_1, \ldots, X_m$ $(m < n)$ is an orthonormal basis of Δ, then the vector fields $X_1, \ldots, X_m$ play the same role as ordinary derivatives in the Euclidean case.

The main property of the vector fields $X_1, \ldots, X_m$ is the Hörmander condition, which requires that the generated Lie Algebra has maximum rank at every point. Under this assumption Chow's Theorem ensures that it is possible to connect any couple of points through an integral curve of $X_1, \ldots, X_m$, called horizontal curve. As a consequence it is possible to define a distance $d(x, y)$ as the length of the shortest path (in the g metric)

connecting the two points x and y. Note that $X_1, \ldots, X_m$ are m vector fields on an n-dimensional space: in absence of Hörmander condition it is not possible to connect any couple of points by horizontal curves, so that a distance is not well defined.

In [6] families of constant coefficients horizontal curves starting from the same point are proposed as a model of the neural connectivity structure between cortical cells. Indeed experimental evidence shows that this neural connectivity structure is strongly anisotropic, and its strength is higher between cells having the same orientation. This is why it can be correctly modeled by horizontal integral curves of the sub-Riemannian space.

Aim of this thesis is to develop an analogous model for the motor cortex. Neural data are available, but no geometrical models in terms of differential instruments have been proposed so far, therefore we will refer to sensory areas, and in particular to visual cortex which has been intensively studied with these instruments. Nevertheless the adaptation is not straightforward, since visual area cortical cells respond to an external stimulus and their activity is computed within the cortex. On the contrary, the input of the primary motor area comes from brain higher cortical areas, whereas the output is movement.

The main results on this topic have been obtained by Georgopoulos (see for example [9], [10], [11], [12], [13], [14]). His experiments allow to recognize some features of the functional architecture of the motor cortex. A key observation is that motor cortical cells are sensitive to movement direction. More precisely, electrical response measured on a motor neuron depends on the direction of the movement performed by a precise part of our body. We are interested in cells sensitive to the movement of the hand. Each of these cells gives a maximal response when the direction of movement coincides with a determined direction, called cell's preferred direction (PD). Moreover, motor cortical cells are organized in orientation columns: it has been noted the location of cells with specific PD along histologically identified penetrations and it has been observed a change in PD in penetrations at an angle with anatomical cortical columns. This structure generalizes the one already identified in visual cortex. We will study the hypercolumnar structure at varying the initial position of the arm. The most original result of the thesis consists on finding out that motor neurons PDs are codified by an intrinsic reference system depending on arm position and not by an external (Cartesian) reference system. A proper model for these intrinsic coordinates are the exponential canonical coordinates around a fixed point.

The thesis is organized in four Chapters. In the first one we review some geometric notions and the Hörmander condition, which are necessary to develop the cortex models. In the second Chapter we present the visual cortex model proposed by Citti-Sarti, while Chapters 3 and 4 contain our original

results. In particular, the third Chapter is a selection of the neurophysiological papers needed to describe the model, whereas the last Chapter contains the model of motor cortex.

Contents

Chapter 1

Geometric preliminaries

1.1 Motivations

The functional architecture of the visual cortex is constituted by the properties of neurons and neural connections which are at the basis of neural functionality and perceptual phenomena. In other words we classify cells on the basis of the perceptual phenomena they implement, not on a pure histological basis. In addition the cells generate a sensitive and perceived space which is inherited but do not coincide with external geometrical space generated by properties of the objects which surround us. Indeed the perception is mediated by the vision process, as visual illusion prove.

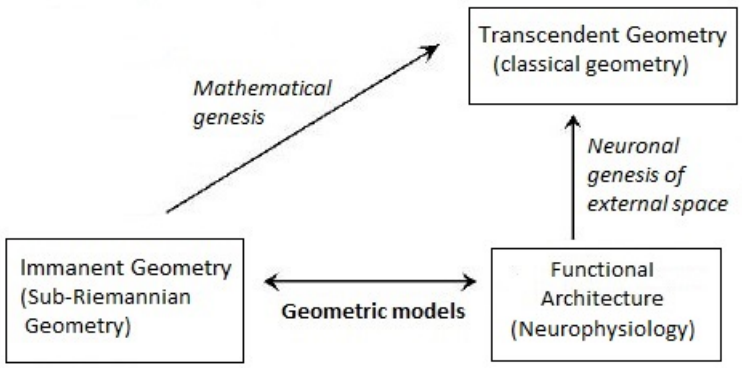

Figure 1.1: General scheme proposed by Petitot [22] to describe the visual cortex Geometry.

According to Petitot ([22]) there is therefore a neuronal-spatial genesis concerning functional architecture and geometric properties of outer space. On the other hand, we will find functional architecture geometric models, or better, geometric models implementing precise cortical structures. It is essential to distinguish these two levels of geometry. To clarify the distinction

we can consider the classical philosophical opposition between *immanence* and *transcendence*. The geometry of the functional architectures is immanent to the cortex, internal, local and its global structures are obtained by integration and coherence of its local data. On the contrary, the geometry of the sensible space is transcendent in the sense that it concerns the external world.

The aim of this chapter is to introduce the mathematical instruments able to describe the immanent geometry of the visual and motor cortex.

1.2 A review of Vector Bundles and Lie Groups

We need to recall some key concepts to understand Sub-Riemannian geometry (see for example [19], [20] and [8]).

1.2.1 Vector bundles

Definition 1.1. A *(differentiable) vector bundle* of rank n consists of a quadruple (E, M, F, π) such that:

1. E and M are differentiable manifolds, called respectively *total space* and *base* of the vector bundle;
2. F is an n-dimensional (real) vector space, called *fiber* of the vector bundle;
3. $\pi : E \to M$ is a differentiable map, called structural *projection* of the vector bundle;
4. $E_x := \pi^{-1}(x)$ for every $x \in M$ is isomorphic to F;
5. the following local requirement is satisfied:
   for every $x \in M$, there exists a neighborhood U and a diffeomorphism
   $$\varphi : \pi^{-1}(U) \to U \times F$$
   with the property that for every $y \in U$
   $$\varphi_y := \varphi_{|E_y} : E_y \to \{y\} \times F$$
   is a vector space isomorphism, i.e. a bijective linear map. Such a pair (φ, U) is called a *bundle chart*.

Remark 1.1. It is important to point out that a vector bundle is by definition locally, but not necessarily globally, a product of base and fiber. A vector bundle which is isomorphic to $M \times \mathbb{R}^n$ ($n =$ rank) is called *trivial*.

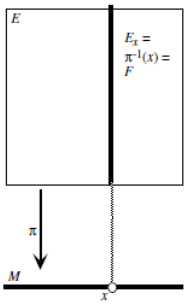

Figure 1.2: Figure taken by [22]. General scheme of a vector bundle of total space E, base M and fiber F (see Definition 1.1). Above each point $x \in M$ the fiber $E_x := \pi^{-1}(x)$ is isomorphic to F.

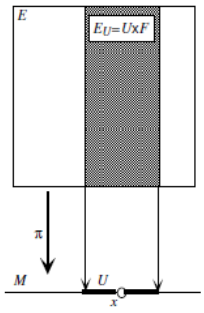

Figure 1.3: The locally product of base and fiber's vector bundle. For every $x \in M$ there exists a neighborhood U such that $E_U := \pi^{-1}(U)$ is isomorphic to $U \times F$.

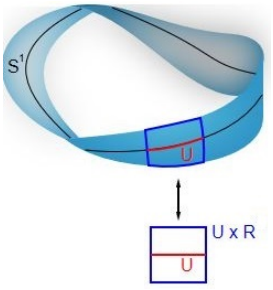

Figure 1.4: The Möbius strip as a vector bundle of rank 1.

Example 1.1. The Möbius strip is a line bundle (a vector bundle of rank 1) over the 1-sphere S^1. Locally around every point in S^1, it is isomorphic to $U \times \mathbb{R}$ (where U is an open arc including the point), but the total bundle is different from $S^1 \times \mathbb{R}$ (which is a cylinder instead).

Remark 1.2. A vector bundle may be considered as a family of vector spaces (all isomorphic to a fixed model $\mathbb{R}^n$) parametrized (in a locally trivial number) by a manifold.

Definition 1.2. Let (E, M, F, π) be a vector bundle. A *section* of E is a differential map $s : M \to E$ with $\pi \circ s = id_M$. The space of sections of E is denoted by $\Gamma(E)$.

An example of a vector bundle above is the tangent bundle TM of a differentiable manifold M.

Definition 1.3. A section of the tangent bundle TM of M is called a *vector field* on M.

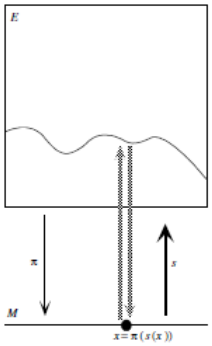

Figure 1.5: A section of a vector bundle defined on an open set U of M associates at each point $x \in U$ a value $s(x)$ in the fiber E_x above x.

Remark 1.3. The projection map π defines a function that at each point in E associates a single point in M. Conversely, a section in a vector bundle just selects one of the points in each fiber.

Remark 1.4. In a trivial vector bundle $E = M \times F$, a section defined on open set $U \subset M$ is nothing more than an application $s : U \to F$.

Another fundamental definition for this thesis is the following one.

Definition 1.4. A *fiber bundle* is a quadruple (E, M, G, π) defined by two differentiable manifolds M and E, a topological space G, and a projection π. E and M are called, respectively, *total space* and *base space*. The total space is locally described as a cartesian product $E = M \times G$, meaning that at every point $m \in M$ is associated a whole copy of the group G, called the *fiber*. The function π is a surjective continuous map, which locally acts as follows

$$\begin{aligned} \pi : M \times G &\longrightarrow M \\ (m, g) &\longmapsto m, \end{aligned}$$

where g is an element of G. Moreover, a function

$$\begin{aligned} \Sigma : M &\longrightarrow M \times G \\ m &\longmapsto (m, \bar{g}), \end{aligned}$$

defined on the base space M with values in the fiber bundle is called a *section* of the fiber bundle. In other words a section is the selection of a point on a fiber.

1.2.2 Integral curves of Vector Fields

Let M be a differentiable manifold, X a vector field on M, that is, as we saw in the previous section, a smooth section of the tangent bundle TM. As a result, X can be represented as

$$X = \sum_{k=1}^{n} a_k \partial_k, \tag{1.1}$$

where a_k are smooth. If I is the identity map $I(\xi) = \xi$, then it is possible to represent a vector field with the same components as the differential operator X in the form

$$XI(\xi) = (a_1, \ldots, a_n). \tag{1.2}$$

Sometimes the vector field and the differential operator are identified and we will not distinguish them unless convenience reasons occur.

XI then defines a first order differential equation:

$$\dot{\gamma} = XI(\gamma).$$

With the identification previously introduced we will simply denote: $\dot{\gamma} = X(\gamma)$. This means that for each $\xi \in M$ one wants to find an open interval $J = J_\xi$ around $0 \in \mathbb{R}$ and a solution of the following differential equation for $\gamma : J \to M$

$$\begin{cases} \dfrac{d\gamma}{dt}(t) = X(\gamma(t)) \quad \text{for } t \in J \\ \gamma(0) = \xi. \end{cases} \tag{1.3}$$

This system has a unique solution by the Cauchy-Peano-Picard theorem:

Lemma 1.1. *For each point $\xi \in M$, there exists an open interval $J_\xi \subset \mathbb{R}$ with $0 \in J_\xi$ and a smooth curve*

$$\gamma_\xi : J_\xi \to M \tag{1.4}$$

solution of problem (1.3).

Definition 1.5. If γ_ξ is the solution of the system (1.3) defined in (1.4) we will denote

$$\exp(tX)(\xi) := \gamma_\xi(t).$$

Since the solution also depends smoothly on the initial point ξ by the theory of ODEs, we furthermore obtain

Lemma 1.2. *For each point $\eta \in M$, there exists an open neighborhood U of η and an open interval J with $0 \in J$, with the property that:*

1. *for all $\eta \in U$, the curve γ_ξ solution of* (1.3) *is defined on J;*
2. *the map $(t, \xi) \mapsto \gamma_\xi(t)$ from $J \times U$ is smooth.*

Now we can show a crucial definition for this paper:

Definition 1.6. The map $(t, \xi) \mapsto \gamma_\xi(t)$ is called the *local flow* of the vector field X. The curve γ_ξ is called the *integral curve* of X through ξ.

For fixed ξ, one thus seeks a curve through ξ whose tangent vector at each point coincides with the value of X at this point, namely, a curve which is always tangent to the vector field X. Hence we study the regularity of the exponential map defined in Definition 1.5 with respect to the variable ξ:

Theorem 1.3. *We have*

$$\exp(tX)\exp(sX)(\xi) = \exp((t+s)X)(\xi) \quad \text{if } s, t, t+s \in J_\xi. \tag{1.5}$$

If $\exp(tX)$ is defined on $U \subset M$, it maps U diffeomorphically onto its image.

Proof. We have

$$\dot{\gamma}_\xi(t+s) = X(\gamma_\xi(t+s)),$$

hence

$$\gamma_\xi(t+s) = \gamma_{\gamma_\xi(s)}(t).$$

Starting from ξ, at time s one reaches the point $\gamma_\xi(s)$, and if one proceeds a time t further, one reaches $\gamma_\xi(t+s)$. One therefore reaches the same point if one walks from ξ on the integral curve for a time $t+s$, or if one walks a time t from $\gamma_\xi(s)$. This shows (1.5). Inserting $t = -s$ into (1.5) for $s \in J_\xi$, we obtain

$$\exp(-sX)\exp(sX)(\xi) = \exp(0X)(\xi) = \xi.$$

Thus, the map $\exp(-sX)$ is the inverse of $\exp(sX)$, and the diffeomorphism property follows. □

Corollary 1.4. *Each point in M is contained in precisely one integral curve.*

Proof. Let $\xi \in M$. Then $\xi = \gamma_\xi(0)$, and so it is trivially in an integral curve. Assume now that $\xi = \gamma_\eta(t)$. Then, by Theorem 1.3 , $\eta = \gamma_\xi(-t)$. Thus, any point whose flow line passes through ξ is contained in the same flow line, namely the one starting at ξ. Therefore, there is precisely one flow line going through ξ. □

Remark 1.5. We observe that flow lines can reduce to single points: this happens for those points for which $X(\xi) = 0$. Also, flow lines in general are not closed even if the flow exists for all $t \in \mathbb{R}$. Namely, the points $\lim_{t\to\pm\infty} \gamma_\xi(t)$ (assuming that these limits exist) need not to be contained in the flow line through ξ.

1.2.3 Lie Algebras

Definition 1.7. Let X, Y be vector fields on a differentiable manifold M. Their *Lie bracket*, or *commutator*, is defined by the vector field

$$[X, Y] = XY - YX.$$

The Lie Bracket is a measurement of the non-commutativity of the vector fields: it is defined as the difference of applying them in reverse order. In particular $[X, Y]$ is identically 0 if X and Y commute.

Lemma 1.5. *If X and Y are vector fields on a differentiable manifold M, then their Lie bracket $[X, Y]$ is linear over $\mathbb{R}$ in X and Y. For a differentiable function $f : M \to \mathbb{R}$, we have $[X, Y] f = X(Y(f)) - Y(X(f))$.*
Furthermore,

$$[X, X] = 0$$

for any vector field X and the Jacobi identity holds:

$$[[X, Y], Z] + [[Y, Z], X] + [[Z, X], Y] = 0$$

for any three vectors fields X, Y, Z.

Proof. In local coordinates with $X = \sum_{i=1}^n a_i \partial_{x_i}$ and $Y = \sum_{j=1}^n b_j \partial_{x_j}$, we have

$$[X, Y] f = \sum_{i=1}^n a_i \partial_{x_i} \left(\sum_{j=1}^n b_j \partial_{x_j} f \right) - \sum_{j=1}^n b_j \partial_{x_j} \left(\sum_{i=1}^n a_i \partial_{x_i} f \right) = X(Y(f)) - Y(X(f))$$

and this is linear in f, X, Y. This implies the first three claims. The Jacobi identity follows by direct computations. □

We add the following

Remark 1.6. If X and Y are first order operators:

$$X = a_1\partial_1 + \cdots + a_n\partial_n,$$
$$Y = b_1\partial_1 + \cdots + b_n\partial_n$$

a simple computation ensures that

$$[X,Y] = XY - YX = Xb_1\partial_1 + \cdots + Xb_n\partial_n - Ya_1\partial_1 - \cdots - Ya_n\partial_n$$

is a first derivative. Therefore the Lie bracket is a first order differential operator obtained by the difference of two second derivatives. Hence the set of C^∞ first order differential operators is closed with respect to the bracket operation.

Definition 1.8. A *Lie algebra* (over $\mathbb{R}$) is a real vector space V equipped with a bilinear map $[\cdot,\cdot] : V \times V \to V$, the Lie bracket, satisfying:

1. $[X,X] = 0$ for all $X \in V$;
2. $[[X,Y],Z] + [[Y,Z],X] + [[Z,X],Y] = 0$ for all $X,Y,Z \in V$.

It follows the fundamental

Corollary 1.6. *The space of vector fields on a differentiable manifold, equipped with the Lie bracket, is a Lie Algebra.*

Definition 1.9. A homomorphism between two Lie algebras is a linear map $\phi : V \to V'$ that is compatible with the respective Lie brackets:

$$\phi[X,Y] = [\phi(X), \phi(Y)], \quad \text{for all } X,Y \in V.$$

Lie algebras automorphisms, epimorhisms and isomorphisms are defined in obvious way.

Examples of Lie algebras are:

- the Euclidean space $\mathbb{R}^n$, with the Lie bracket defined by $[u,v] = 0$ for all $u,v \in \mathbb{R}^n$ is a Lie algebra;
- the set of square matrices $n \times n$, with determinant different from 0, namely $Gl(n,\mathbb{R})$ is a Lie Algebra with the Lie bracket defined by $[A,B] = AB - BA$ for all $A,B \in Gl(n,\mathbb{R})$;
- if V is a real vector space, the set of all endomorphisms of V, $End(V)$ is a Lie Algebra with the Lie bracket defined by $[f,g] = f \circ g - g \circ f$ for all $f,g \in End(V)$. Moreover, if V has dimension n, chosen a basis for V, $Gl(n,\mathbb{R})$ is isomorphic to $End(V)$ as Lie Algebra.
- If M is a smooth manifold, the set of C^∞ vector fields defined on M is a Lie Algebra with the Lie bracket provided in Definition 1.7.

1.2.4 Lie Groups

In this section we provide some basic definitions of the Lie group theory, as it is an essential framework utilized in this thesis. All definitions can be found in standard mathematical textbooks (for example [8] and [19]).

Definition 1.10. A *Lie group* is a group G carrying the structure of a differentiable manifold or, more generally, of a disjoint union of finitely many differentiable manifolds for which the following maps are differentiable:

$$\begin{aligned} G \times G \to G \quad &\text{(multiplication)} \\ (g, h) \mapsto g \cdot h \end{aligned}$$

and

$$\begin{aligned} G \to G \quad &\text{(inverse)} \\ g \mapsto g^{-1}. \end{aligned}$$

Definition 1.11. A Lie group G *acts on a differentiable manifold* M *from the left* if there is a differentiable map

$$\begin{aligned} G \times M &\to M \\ (g, x) &\mapsto gx \end{aligned}$$

that respects the Lie group structure of G in the sense that

$$g\,(hx) = (g \cdot h)\,x \quad \text{for all } \; g, h \in G, \; x \in M.$$

An action from the right is defined analogously.

Examples of Lie Groups are:

- the Euclidean space $\mathbb{R}^n$, with the usual sum as group law;
- the set of square matrices $n \times n$, with determinant different from 0. In this set we consider the standard product of matrices, and the existence of inverse is ensured by the condition on the determinant. This group is not commutative;
- the circle S^1 of angles mod 2π, with the standard sum of angles.

Now we will see Lie algebras of Lie groups.

Definition 1.12. Let G be a Lie group. For $g \in G$, we have the *left translation*

$$\begin{aligned} L_g : G &\to G \\ h &\mapsto gh \end{aligned}$$

and the *right traslation*

$$\begin{aligned} R_g : G &\to G \\ h &\mapsto hg. \end{aligned}$$

L_g and R_g are diffeomorphism of G, $(L_g)^{-1} = L_{g^{-1}}$.

We recall that if $\phi : M \to N$ is a differentiable map between two differentiable manifolds, the differential $d\phi$ at point $m \in M$ is a linear map between the tangent bundles T_pM and $T_{\phi(p)}N$ denoted by ϕ_{p^*}.

Definition 1.13. A vector field X on a Lie group G is called *left invariant* if for all $g, h \in G$

$$L_{g*}X(h) = X(gh),$$

namely

$$L_{g*}X = X \circ L_g.$$

We will see in Definition 1.14 that it is possible to associate to a group the Lie algebra of its left invariant vector fields, and we need to state some preliminary results.

Lemma 1.7. *Let $\phi : M \to N$ be a diffeomorphism between two differentiable manifolds and X, Y vector fields on M. Then*

$$[\phi_* X, \phi_* Y] = \phi_* [X, Y].$$

Thus, ϕ_* induces a Lie algebra isomorphism.

Theorem 1.8. *Let G be a Lie group and e the unit element of G. For every $V \in T_eG$,*

$$X(g) := L_{g^*} V$$

defines a left invariant vector field on G, and we thus obtain an isomorphism between T_eG and the space of left invariant vector fields on G.

By the previous Lemma, for $g \in G$ and vector fields X, Y

$$[L_{g^*} X, L_{g^*} Y] = L_{g^*} [X, Y].$$

Consequently, the Lie bracket of left invariant vector fields is left invariant itself, and the space of left invariant vector fields is closed under the Lie bracket and hence forms a Lie subalgebra of the Lie algebra of all vector fields on G (Corollary 1.6). From Theorem 1.8, we obtain

Corollary 1.9. *Let G be a Lie group and e the unit element of G. Then T_eG carries the structure of a Lie algebra.*

Definition 1.14. *The Lie algebra* $\mathfrak{g}$ *of a Lie group* G is the vector space T_eG equipped with the Lie algebra structure of Corollary 1.9.

Intuitively the Lie algebra associated to a Lie group encodes its differential structure, and it is identified as the tangent space at the "origin".

In analogy to the Definition of vector bundle where the fiber is a vector space we now define a principal fiber bundle as one where the fiber is a Lie group. This structure will be intensively used in the description of the visual and motor cortex.

Definition 1.15. Let G be a Lie group. A *principal G-bundle* consists of a fiber bundle (E, M, G, π), with an action of G on E satisfying:

1. G acts on E from the right: $(q, g) \in E \times G$ is mapped to $qg \in E$, and $qg \neq q$ for $g \neq e$. The G-action then defines an equivalence relation on E:
$$p \sim q \Leftrightarrow \exists g \in G : \; p = qg.$$

2. M is the quotient of E by this equivalence relation, and $\pi : E \to M$ maps $q \in E$ to its equivalence class. By 1., each fiber $\pi^{-1}(x)$ can then be identified with G.

3. E is locally trivial in the following sense:
for each $x \in M$ there exist a neighborhood U of x and a diffemorphism
$$\varphi : \pi^{-1}(U) \to U \times G$$
of the form $\varphi(p) = (\pi(p), \psi(p))$ which is G-equivariant, namely $\varphi(pg) = (\pi(p), \psi(p)\, g)$ for all $g \in G$.

1.3 Riemannian metrics

We want to give a brief overview to Riemannian metric structures on differentiable manifolds.

Definition 1.16. A *Riemannian metric* on a differentiable manifold M is given by a scalar product on each tangent space T_pM which depends smoothly on the base point p.
A *Riemannian manifold* is a differentiable manifold, equipped with a Riemannian metric.

In order to understand the concept of a Riemannian metric, we need to study local coordinate representations and the transformation behavior of these expressions.

Thus, let $x = \left(x^1, \ldots, x^n\right)$ be local coordinates. In these coordinates, a metric is represented by a positive definite, symmetric matrix

$$\left(g_{ij}\left(x\right)\right)_{i,j=1,\ldots,n}$$

($g_{ij} = g_{ji}$ for all i, j, $g_{ij}\xi^i\xi^j > 0$ for all $\xi = \left(\xi^1, \ldots, \xi^n\right) \neq 0$), where the coefficients depend smoothly on x.

The product of two tangent vectors $v, w \in T_pM$ with coordinate representations $\left(v^1, \ldots, v^n\right)$ and $\left(w^1, \ldots, w^n\right)$ (i.e. $v = \sum_{i=1}^n v^i \frac{\partial}{\partial x^i}, w = \sum_{j=1}^n w^j \frac{\partial}{\partial x^j}$) then is

$$\langle v, w\rangle := \sum_{i,j=1}^{n} g_{ij}\left(x\left(p\right)\right) v^i w^j. \tag{1.6}$$

In particular, $\left\langle \frac{\partial}{\partial x^i}, \frac{\partial}{\partial x^j}\right\rangle = g_{ij}$.

Similarly, the lenght of v is given by

$$|v| := \langle v, v\rangle^{\frac{1}{2}}.$$

Example 1.2. The simplest example of a Riemannian metric of course is the Euclidean one. Indeed, for $v = \left(v^1, \ldots, v^n\right)$, $w = \left(w^1, \ldots, w^n\right) \in T_x\mathbb{R}^n$, the Euclidean scalar product is simply

$$\sum_{i,j=1}^{n} \delta_{ij} v^i w^j = \sum_{i=1}^{n} v^i w^i,$$

where δ_{ij} is the standard Kronecker symbol.

Let now $[a, b]$ be a closed interval in $\mathbb{R}$, $\gamma : [a, b] \to M$ a smooth curve, where "smooth" means "of class $\mathcal{C}^\infty$".
The length of γ then is defined as

$$L\left(\gamma\right) := \int_a^b \left|\frac{d\gamma}{dt}\left(t\right)\right| dt.$$

Of course this expression can be computed in local coordinates. Working with the coordinates $\left(x^1\left(\gamma\left(t\right)\right), \ldots, x^d\left(\gamma\left(t\right)\right)\right)$ we use the abbreviation

$$\dot{x}^i\left(t\right) := \frac{d}{dt}\left(x^i\left(\gamma\left(t\right)\right)\right).$$

Then

$$L\left(\gamma\right) := \int_a^b \sqrt{\sum_{i,j=1}^{n} g_{ij}\left(x\left(\gamma\left(t\right)\right)\right) \dot{x}^i\left(t\right) \dot{x}^j\left(t\right)} dt.$$

On a Riemannian manifold M, the *distance* between two points p, q can be defined:

$$d(p,q) := \inf\{L(\gamma) : \gamma : [a,b] \to M \text{ piecewise smooth curve with } \gamma(a) = p, \gamma(b) = q\}.$$

Remark 1.7. Any two points $p, q \in M$ can be connected by a piecewise smooth curve, and $d(p,q)$ therefore is always defined. Namely, let

$$E_p := \{q \in M : p \text{ and } q \text{ can be connected by a piecewise smooth curve}\}.$$

With the help of local coordinates one sees that E_p is open. But then also $M \setminus E_p = \bigcup_{q \notin E_p} E_q$ is open. Since M is connected and $E_p \neq \emptyset$ ($p \in E_p$), we conclude $M = E_p$.

In [19] can be found the proof that the distance function satisfies the usual axoms:

(i) $d(p,q) \geq 0$ for all p, q and $d(p,q) > 0$ for all $p \neq q$,

(ii) $d(p,q) = d(q,p)$,

(iii) $d(p,q) \leq d(p,r) + d(r,q)$ (triangle inequality) for all points $p, q, r \in M$.

1.4 Hörmander vector fields and Sub-Riemannian structures

First of all we introduce some definitions we will widely use in this paper (see for example [6]). In general we will denote ξ the points in $\mathbb{R}^n$.

Let us now give the following definition:

Definition 1.17. Let M be a differentiable manifold of dimension n. We call *distribution* Δ a subbundle of the tangent bundle. Δ is a *regular distribution* if at every point $\xi \in M$ there exists a neighbourhood $U_\xi \subset M$ of ξ and m linearly independent smooth vector fields $X_1, \cdots, X_m$ defined on U_ξ such that for any point $\eta \in U_\xi$

$$Span\left(X_{1_{|\eta}}, \ldots, X_{m_{|\eta}}\right) = \Delta_\eta \subseteq T_\eta M.$$

If the distribution is regular, the vector space Δ_η, is called *horizontal tangent space* at the point η. The distribution Δ defined in this way is called *horizontal tangent bundle* of rank m.

In the sequel we will always consider the following generalization of Riemannian manifolds.

Definition 1.18. We will call *degenerate Riemannian manifold* a triple (M, Δ, g), where

1. M is a differentiable manifold,
2. Δ is an horizontal tangent bundle of rank m
3. g is a metric defined on Δ

Definition 1.19. The metric g induces on the space a scalar product and a norm called respectively *horizontal scalar product* and *horizontal norm*, as in definition (1.6).

Remark 1.8. Let us explicitly note that in order to give the analogous definition of scalar product in this setting, we have used the regularity of the distribution.

We stress the fact that in a Riemannian manifold the scalar product is defined on the whole tangent space of each point of the manifold, whereas in a degenerate Riemannian manifold the scalar product is defined in a precise subset of the tangent space.

For each ξ and each vector field X_j defined on U_ξ will be represented as

$$X_j := \sum_{k=1}^{n} a_{jk}\partial_k, \quad j = 1, \dots, m, \tag{1.7}$$

in U_ξ with $m < n$ and a_{jk} of class $\mathcal{C}^\infty$.

Remark 1.9. Since we are interested in local properties of the vector fields, we will often assume that the vector fields $X_1, \cdots, X_m$ are defined on the whole manifold M. If the metric is not explicitly defined, we will implicitly choose the metric g which makes the basis $X_1, \dots, X_m$ an orthonormal basis.

As we have seen in Corollary 1.6, the Horizontal tangent bundle is naturally endowed with a structure of Lie algebra through the bracket. By Remark 1.6, the commutator is a first order vector field obtained as a difference of second order derivatives, so that there is a kind of homogeneity on the second derivative that we will soon analyze.

Definition 1.20. We call *Lie Algebra generated by* $X_1, \dots, X_m$ and denoted as

$$\mathcal{L}(X_1, \dots, X_m)$$

the linear span of the operators $X_1, \dots, X_m$ and their commutators of any order.

We will say that the vector fields

$$\begin{aligned} X_1, \dots, X_m &\text{ have degree 1} \\ [X_i, X_j]_{i,j=1,\dots,m} &\text{ have degree 2} \end{aligned}$$

and define in an analogous way higher order commutators.

Remark 1.10. The degree is not unique, indeed, if we consider the following vector fields in $\mathbb{R}^2 \times S^1$ where the points are denoted as $\xi = (x_1, x_2, \vartheta)$:

$$X_1 = \cos(\vartheta)\,\partial_1 + \sin(\vartheta)\,\partial_2, \quad X_2 = \partial_\vartheta$$

their Lie bracket is $[X_1, X_2] = \sin(\vartheta)\,\partial_1 - \cos(\vartheta)\,\partial_2$ and $X_1 = -[X_2, [X_2, X_1]]$. Thus, X_1 has both degree 1 and 3.

Therefore we call *minimum degree of* $X_j \in \mathcal{L}(X_1, \dots, X_m)$ and denote it as

$$deg(X_j) = \min\{i : X_j \text{ has degree } i\}.$$

Remark 1.11. Since $m < n$, in general

$$\mathcal{L}(X_1, \dots, X_m)$$

will not coincide with the Euclidean tangent plane. If these two spaces coincide, we will say that the Hörmander condition is satisfied as we will see in the next Definition.

Definition 1.21. Let M be a regular manifold of dimension n and let $(X_j)_{j=1,\dots,m}$ be a family of smooth vector fields defined on M. If the condition

$$\mathcal{L}(X_1, \dots, X_m)_{|_\xi} = T_\xi M \simeq \mathbb{R}^n \quad , \forall \xi \in M$$

is satisfied, we say that the vector fields $(X_j)_{j=1,\dots,m}$ satisfy the *Hörmander condition* and they are called *Hörmander vector fields.*

Remark 1.12. If this condition is satisfied at every point ξ we can find a number s such that $(X_j)_{j=1,\dots,m}$ and their commutators of degree smaller or equal to s span the space at ξ. If s is the smallest of such natural numbers, we will say that *the space has step s at the point ξ*. At every point we can select a basis $\{X_j : j = 1, \dots, n\}$ of the space made out of commutators of the vector fields $\{X_j : j = 1, \dots, m\}$. In general the choice of the basis will not be unique, but we will choice a basis such that for every point

$$Q = \sum_{j=1}^{n} deg(X_j)$$

is minima. The value of Q is called *homogeneous dimension* of the space. In general it is not constant, but by simplicity in the sequel we will assume that s and Q are constant in the considered open set. This assumption is always satisfied in a Lie group.

Example 1.3. The simplest example of family of vector fields is the Euclidean one: $X_i = \partial_i$, $i = 1, \dots, m$ in $\mathbb{R}^n$. If $m = n$, then the Hörmander condition holds, while it is trivially violated if $m < n$.

Example 1.4. Let us consider the following vector fields in $\mathbb{R}^3$ where the points are denoted as $\xi = (x, y, z)$ and

$$X_1 = \partial_x + z\partial_y, \quad X_2 = \partial_z.$$

Since $[X_1, X_2] = -\partial_y$, then the Hörmander condition is satisfied.

Example 1.5. If we consider the vector fields in $\mathbb{R}^2 \times S^1$ used in Remark 1.10 as the generators of the Lie algebra, namely

$$X_1 = \cos(\vartheta)\,\partial_1 + \sin(\vartheta)\,\partial_2 \text{ and } X_2 = \partial_\vartheta,$$

their commutator is

$$X_3 = [X_1, X_2] = \sin(\vartheta)\,\partial_1 - \cos(\vartheta)\,\partial_2,$$

which is linearly independent of X_1 and X_2. Therefore, even in this case, X_1, X_2 are Hörmander vector fields

1.4.1 Sub-Riemannian manifolds

Definition 1.22. A *sub-Riemannian manifold* is a degenerate Riemannian manifold (M, Δ, g) such that for every ξ in M there exists a basis $X_1, \cdots, X_m$ of the horizontal tangent bundle Δ in a neighborhood of the point ξ satisfying the Hörmander condition.

Remark 1.13. Let us note that if for every ξ in M there exists a basis $X_1, \cdots, X_m$ of the horizontal tangent bundle Δ in a neighborhood of the point ξ satisfies the Hörmander condition, any other basis satisfies the same condition.

Let's introduce the following fundamental

Definition 1.23. Let (M, Δ, g) be a sub-Riemannian manifold. A curve $\gamma : [0, 1] \to M$ of class $\mathcal{C}^1$ is called *admissible*, or *horizontal*, if and only if $\gamma'(t) \in \Delta_{\gamma(t)}$, $\forall t \in [0, 1]$.

Now the question is: can we define a distance with these horizontal curves? The idea is to define a distance similar to the Riemannian case, but since in the sub-Riemannian setting only integral curves of horizontal vector fields are allowed, we need to ensure that it is possible to connect any couple of points p and q through an horizontal integral curve.

1.4.2 Connectivity property

The aim of this subsection is to prove Chow's Theorem which ensures that if the Hörmander condition holds, then the connectivity property is satisfied; hence it will be possible to define a distance in a sub-Riemannian setting. Let us postpone the theorem after a few examples of vector fields satisfying the connectivity condition.

Example 1.6. In the Euclidean case considered in Example 1.3, if $m = n$, then the Hörmander condition is satisfied, and any couple of points can be joint with an Euclidean integral curve. If m $< n$, when the Hörmander condition is violated, also the connectivity condition fails. Indeed if we start from the origin, with an integral curve of the vectors $X_i = \partial_i$, $i = 1, \dots, m$, we can reach only points with the last $n - m$ components identically 0.

Example 1.7. In the Example 1.4 the Hörmander condition is satisfied. On the other side, it is easy to see that we can connect any point (x, y, z) with the origin through a piecewise regular horizontal curve. It is not resctrictive to assume $x \neq 0$. Indeed, if we call $\tilde{z} = \frac{y}{x}$, the segment $[(0,0,0), (0,0,\tilde{z})]$ is an integral curve of X_2. Then the segment $[(0,0,\tilde{z}), (x,y,\tilde{z})]$ is an integral curve of X_1. Finally the segment $[(x,y,\tilde{z}), (x,y,z)]$ is an integral curve of X_2.

Example 1.8. We already verified that the vector fields described in Remark 1.10 satisfy the Hörmander condition. On the other hand also in this case it is possible to verify directly that any couple of points can be connected by a piecewise regular path.

In section 1.2.2 we introduced the notion of exponential map and integral curves of vector fields. Here we study the properties of this map under the Hörmander condition. Since we are interested in local properties, we will assume that the underlying manifold M coincides with $\mathbb{R}^n$. To avoid misanderstanding we will keep the distinction between the first order differential operator X and the associated vector field XI, using the definition introduced in (1.2). Let us start with the following lemma:

Lemma 1.10. *Let $\Omega \subset \mathbb{R}^n$ be an open set, and let X be a first order differential operator defined on Ω. If $f \in \mathcal{C}^1(\Omega, \mathbb{R})$ and*

$$\begin{cases} \gamma'(t) = XI(\gamma) \\ \gamma(0) = \xi_0 \in \Omega, \end{cases}$$

then

$$\frac{d}{dt}(f \circ \gamma)(t) = (Xf)(\gamma(t)). \tag{1.8}$$

Proof. Considering the notations used in (1.2),

$$\begin{aligned}\frac{d}{dt}\left(f\circ\gamma\right)(t) &= \left\langle \nabla f\left(\gamma\left(t\right)\right), \gamma'\left(t\right)\right\rangle = \left\langle \nabla f\left(\gamma\left(t\right)\right), XI\left(\gamma\left(t\right)\right)\right\rangle = \\ &= \sum_{k=1}^{n} \partial_k f\left(\gamma\left(t\right)\right) a_k\left(\gamma\left(t\right)\right) = \sum_{k=1}^{n} \left(a_k \partial_k f\right)\left(\gamma\left(t\right)\right) = \\ &= \left(Xf\right)\left(\gamma\left(t\right)\right).\end{aligned}$$

□

Remark 1.14. The condition $f \in \mathcal{C}^1\left(\Omega, \mathbb{R}\right)$ can be weakened: it would be enough that f is defined only on γ.

Lemma 1.11. *Let $\Omega \subset \mathbb{R}^n$ be an open set, let X be a first order differential operator of class $\mathcal{C}^2$ defined on Ω. Then, the following estimation holds:*

$$\exp\left(tX\right)\left(\xi\right) = \xi + t\left(XI\right)\left(\xi\right) + \frac{t^2}{2}\left(X^2 I\right)\left(\xi\right) + o\left(t^2\right), \tag{1.9}$$

where the exponential map has been introduced in Definition 1.5.

Proof. The Taylor expansion ensures that

$$\gamma\left(t\right) = \gamma\left(0\right) + t\gamma'\left(0\right) + \frac{t^2}{2}\gamma''\left(0\right) + o\left(t^2\right).$$

Now,

$$\gamma'\left(t\right) = XI\left(\gamma\left(t\right)\right) = \left(\left(XI\right)\circ\gamma\right)\left(t\right),$$

hence

$$\gamma''\left(t\right) = \left(\left(XI\right)\circ\gamma\right)'\left(t\right) = X^2 I\left(\gamma\left(t\right)\right) \quad \text{from (1.8).}$$

Since $\gamma\left(0\right) = \xi$, we obtain

$$\begin{aligned}\gamma'\left(0\right) &= XI\left(\gamma\left(0\right)\right) = \left(XI\right)\left(\xi\right) \\ \gamma''\left(0\right) &= X^2 I\left(\gamma\left(0\right)\right) = \left(X^2 I\right)\left(\xi\right).\end{aligned}$$

Substituting, the assertion is proved. □

From this Lemma, the following Corollary is immediate

Corollary 1.12. *In the same hypothesis as Lemma 1.11, let $f \in \mathcal{C}^2\left(\Omega, \mathbb{R}\right)$. Then, the following estimation holds:*

$$f\left(\exp\left(tX\right)\right)\left(\xi\right) = f\left(\xi\right) + t\left(Xf\right)\left(\xi\right) + \frac{t^2}{2}\left(X^2 f\right)\left(\xi\right) + o\left(t^2\right). \tag{1.10}$$

Now we are closer to prove Chow's Theorem. The idea behind the proof is to get the direction of the commutators to recover all space directions, thanks to Hörmander condition

Lemma 1.13. *Let $\Omega \subset \mathbb{R}^n$ be an open set and let X, Y be differential operators of class $\mathcal{C}^2$ defined on Ω. Then, the following estimation holds:*

$$\begin{aligned} C(t)(\xi) &= \exp(-tY)\exp(-tX)\exp(tY)\exp(tX)(\xi) = \\ &= \exp\left(t^2[X,Y](\xi) + o\left(t^2\right)\right)(\xi). \end{aligned} \tag{1.11}$$

If the coefficients of the vector fields $(X_i)_{i=1,\dots,h}$ are of class $\mathcal{C}^h$, we can define inductively

$$\begin{aligned} &C(t, X_1, \dots, X_h)(\xi) = \\ &= \exp(-tX_1)\, C(t, -X_2, \dots, X_h)\exp(tX_1)\, C(t, X_2, \dots, X_h)(\xi). \end{aligned} \tag{1.12}$$

In this case we have:

$$C(t, X_1, \dots, X_h)(\xi) = \exp\left(t^h [[[[X_1, X_2]\dots]]] + o\left(t^h\right)\right)(\xi).$$

Proof. From Lemma 1.11 we know that

$$\exp(tX)(\xi) = \xi + tXI(\xi) + \frac{t^2}{2}X^2 I(\xi) + o\left(t^2\right).$$

To compute a general second-order Taylor expansion we stop the Taylor expansion of $YI(\exp(tX)(\xi))$ to the first order:

$$YI\left(\xi + tXI(\xi) + \frac{t^2}{2}X^2 I(\xi) + o\left(t^2\right)\right) = YI(\xi) + tXYI(\xi) + o(t).$$

Hence

$$\begin{aligned} &\exp(tY)\exp(tX)(\xi) = \exp(tY)\left(\xi + tXI(\xi) + \frac{t^2}{2}X^2 I(\xi) + o\left(t^2\right)\right) = \\ =&\xi + tXI(\xi) + \frac{t^2}{2}X^2 I(\xi) + o\left(t^2\right) + \\ &+ tYI(\xi) + t^2 XYI(\xi) + \frac{t^2}{2}Y^2 I(\xi) + o\left(t^2\right) = \\ =&\xi + t\left(XI(\xi) + YI(\xi)\right) + \frac{t^2}{2}\left(X^2 I(\xi) + 2XYI(\xi) + Y^2 I(\xi)\right) + o\left(t^2\right). \end{aligned}$$

Applying $\exp(-tX)$ we obtain

$$\begin{aligned} &\exp(-tX)\exp(tY)\exp(tX)(\xi) = \\ =&\xi + tYI(\xi) + \frac{t^2}{2}\left(2[X,Y]I(\xi) + Y^2 I(\xi)\right) + o\left(t^2\right). \end{aligned}$$

Finally

$$\exp(-tY)\exp(-tX)\exp(tY)\exp(tX)(\xi) = \xi + t^2[X,Y]I(\xi) + o\left(t^2\right).$$

The second assertion can be proved by induction, using the same ideas. □

Theorem 1.14 (Chow's theorem).
Let $\Omega \subset \mathbb{R}^n$ be an open and connected set and let $X_1, \dots, X_m$ be smooth differential operators defined on Ω. If the Hörmander condition is satisfied, then any couple of points in Ω can be joint with a piecewise $\mathcal{C}^1$ horizontal curve.

Proof. We make the choice of basis described in Remark 1.12 and assume that

$$X_i = \left[X_{j_1}, \left[\dots, \left[X_{j_{i-1}}, X_{j_i}\right]\right]\right],$$

for suitable indices j_i. Let us now fix t, sufficiently small and assume that it is positive (the proof is analogous, changing the order of vector fields if $t < 0$) and let us call

$$C_i(t) = C\left(t^{\frac{1}{deg(X_i)}}, X_{j_1}, \dots, X_{j_i}\right).$$

By the previous Lemma

$$\frac{d}{dt} C_i(t)_{|_{t=0}} = X_i \quad , \forall i = 1, \dots, n.$$

For every $\xi \in \Omega$ we define

$$\tilde{C}(t)(\xi) = \prod_{i=1}^{n} C_i(t_i)(\xi).$$

The Jacobian determinant of $\tilde{C}$ with respect to t is the determinant of $(X_i)_{i=1,\dots,n} = (a_{i,j})_{i,j=1,\cdots,n}$, if the vector fields are represented as in (1.7). So that it is different from 0. Hence the map $\tilde{C}(t)$ is a local diffeomorphism, and the connectivity property is locally proved. Thanks to this local diffemorphism we can say that

$$\forall \xi \in \Omega, \ \exists r > 0 : \ \forall \eta \in B(\xi, r), \tag{1.13}$$

$$\xi \text{ and } \eta \text{ are connected by piecewise regular horizontal curves.}$$

Finally, we extend this connection to the whole Ω. Let's fix $\xi_0 \in \Omega$ and consider the following Ω subset:

$$A = \{\eta : \eta \text{ is connected to } \xi_0 \text{ by a piecewise regular horizontal curve}\}.$$

A is open, indeed, if $\xi \in A$, ξ is connected to ξ_0 by piecewise regular horizontal curves. From (1.13) we know that $\exists r > 0 : \ \forall \eta \in B(\xi, r)$, η is connected to ξ by piecewise horizontal curves. In this way the whole $B(\xi, r) \subseteq A$, hence A is open.

Let's prove A is closed. Let (ξ_n) be a sequence in A such that $\xi_n \longrightarrow \xi$, $\xi \in \Omega$. From (1.13) we know that $\exists r > 0 : \ \forall \eta \in B(\xi, r)$, η is connected

to ξ by piecewise regular horizontal curves. Since $\xi_n \longrightarrow \xi$, $\exists \bar{n}$ such that $\forall n \geq \bar{n}$, $\xi_n \in B(\xi, r)$. Therefore, $\xi_{\bar{n}}$ is connected to ξ by piecewise regular horizontal curves, but $\xi_{\bar{n}} \in A$, thus $\xi_{\bar{n}}$ connects to ξ_0 by piecewise regular horizontal curves. Then there is a piecewise regular horizontal curve connecting ξ_0 to ξ, in this way we have proved that $\xi \in A$, hence A is closed. Since $A \neq \emptyset$ and it is open and closed in Ω which is connected, we conclude that $A = \Omega$. □

1.4.3 Control distance

If the connectivity property is satisfied, it is possible to give the definition of distance of the space. If we choose the Euclidean metric on the horizontal tangent bundle, we can call length of any horizontal curve γ

$$L(\gamma) = \int_0^1 \left|\gamma'(t)\right| dt,$$

where $|\cdot|$ denotes the horizontal norm introduced in Definition 1.19. Consequently, we can define a distance as:

$$d(\xi, \xi_0) = \inf\{L(\gamma) : \gamma \text{ is an horizontal curve connecting } \xi \text{ and } \xi_0\}. \quad (1.14)$$

This distance is even called *Carnot-Caratheodory distance*. Let us now give a precise estimate of this distance.

As a consequence of Hörmander condition we can locally represent any vector in the form

$$X = \sum_{j=1}^{n} e_j X_j.$$

The norm $\sqrt{\sum_{j=1}^{m} |e_j|^2}$ is equivalent to the horizontal norm expressed in Definition 1.19. We can extend it as a homogeneous norm on the whole space setting:

$$\|e\| = \left(\sum_{j=1}^{n} |e_j|^{\frac{Q}{deg(X_j)}} \right)^{\frac{1}{Q}}, \quad (1.15)$$

where Q has been defined in Remark 1.12.
Since the exponential mapping is a local diffeomorphism, we give the following

Definition 1.24. If $\xi_0 \in \Omega$ is fixed, we define *canonical coordinates of* ξ *around a fixed point* ξ_0, the coefficients e such that

$$\xi = \exp\left(\sum_{j=1}^{n} e_j X_j \right)(\xi_0). \quad (1.16)$$

We only enunciate that this representation can be used to give another characterization of the distance

Proposition 1.15. *The distance defined in* (1.14) *is locally equivalent to*

$$d_1(\xi, \xi_0) = \|e\|,$$

where e are the canonical coordinates of ξ around ξ_0 and $\|\cdot\|$ is the homogeneous norm defined in 1.15.

1.4.4 Riemannian approximation of the metric

In Definition 1.19 we introduced an horizontal norm only on the horizontal tangent plane. We can extend it to a Riemannian norm all the tangent space as follows: for every $\varepsilon > 0$ we locally define

$$\begin{cases} X_j^\varepsilon = X_j, & j = 1, \dots, m \\ X_j^\varepsilon = \varepsilon X_j, & j > m. \end{cases}$$

The family $\left(X_j^\varepsilon\right)_{j=1,\dots,n}$ formally tends to the family $(X_j)_{j=1,\dots,m}$ as $\varepsilon \to 0$. We call Riemannian approximation of the metric g the Riemannian metric g_ε which makes the vector fields orthonormal. Clearly g_ε restricted to the horizontal plane coincide with the Horizontal metric. The geodesic distance associated to g_ε is denoted d_ε, while the ball in this metrics of center ξ_0 and radius r will be denoted

$$B_\varepsilon(\xi_0, r) = \{\xi : d_\varepsilon(\xi, \xi_0) < \varepsilon\}.$$

The distance d_ε tends to the distance d defined in (1.14) as ε goes to 0.

1.5 Sub-Riemannian geometries as models

Sub-Riemannian geometry (also known as Carnot geometry in France, and non-holonomic Riemannian geometry in Russia) has been a full research domain from the 80's, with motivations and ramifications in several parts of pure and applied mathematics.
Sub-Riemannian geometry is a generalization of Riemannian geometry. Roughly speaking, a sub-Riemannian manifold is a Riemannian manifold together with a constrain on admissible direction of movements.

1.5.1 Examples from mathematics and physics

Sub-Riemannian geometry models various structures, from control theory to mechanics, from bio-medicine to quantum phases, from robots to falling cats! In this phase we just want to give hints as examples of the previous

sentence "constrain on admissible direction of movements". This fact as a crucial role in all models.

- *Control theory* is an interdisciplinary branch of engineering and mathematics that deals with the behavior of dynamical systems. The usual objective is to control a system, in the sense of finding, if possible, the trajectories to reach a desired state and do it in an optimal way. Sub-Riemannian geometry follows the same setting of considering systems that are controllable with optimal trajectories and study this spaces as metric spaces. Many of the theorems in sub-Riemannian geometry can be formulated and prove in the more general settings of control theory. For example, the sub-Riemannian Theorem by Chow has more general statement in geometric control theory.

- Theoretical physics defines most mechanical systems by a kinetic energy and a potential energy. Gauge theory also know as the geometry of principal bundles with connections studies systems with physical symmetries, i.e., when there is a group acting on the configuration space by isometries. Most of the times it will be easier to understand the dynamics up to isometries, successively one has to study the "lift" of the dynamics into the initial configuration space. Such lifts will be subject to a sub-Riemannian restriction. The formalism of principal bundles with connections is well presented by the example of the *fall of a cat*. A cat, dropped from upside down, will land on its self. The reason of this ability is the good flexibility of the cat in changing its shape.

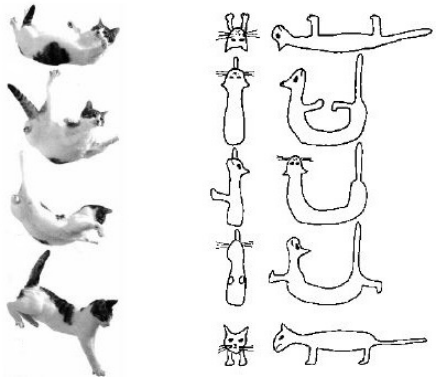

Figure 1.6: The cat spins itself around and right itself.

If we call M the set of all the possible configurations in the 3D space of a given cat and S the set of all the shapes that a cat can assume,

we suppose both M and S are manifolds of dimension quite huge. A position of a cat is just its shape plus its orientation in space. Otherwise said, the group of isometries $G := \mathrm{Isom}\left(\mathbb{R}^3\right)$ of the Euclidean 3D space acts on M and the shape space is just the quotient of the action $\pi : M \to M/G = S$.
The key fact is that the cat has complete freedom in deciding its shape $\sigma(t) \in S$ at each time t. However, during the fall, each strategy $\sigma(t)$ of changing shapes will give as a result a change in configurations $\tilde{\sigma}(t) \in M$. The curve $\tilde{\sigma}(t)$ satisfies $\pi(\tilde{\sigma}) = \sigma$. Moreover the lifted curve is unique: it has to satisfy the constrain given by the "natural mechanical connection". In other words, the cat can choose to vary its shape from the standard normal shape into the same shape giving as a result a change in configuration: the legs were initially toward the sky, then they are toward the floor.

- *Parking a car or riding a bike.* The configuration space is 3-dimensional: the position in the 2-dimensional street plus the angle with respect to a fixed line. However, the driver has only two degree of freedom: turning and pushing, yet we can move the car to any position we like.

- In *robotics* the mechanisms, as for example the arm of a robot, are subjected to constrain of movements but do not decrease the manifold of positions. Similar is the situation of satellites. One should really think about a satellite as a falling cat: it should choose properly its strategy of modifying the shape to have the necessary change in configuration. Another similar example is the case of an astronaut in outer space.

A fundamental example for this thesis concerns neurophysiological research: next Chapter will be devoted to the mathematical modeling of visual cortical space. The focus is on the structure of the visual cortex, which is responsible for the functionality of the visual cortex itself. This model will be the main inspiration for the motor cortex mathematical model.

Chapter 2

A sub-Riemannian model of the visual cortex

The aim of this Chapter is to provide a differential model of primary visual cortex (V1). In the the first of the Chapter we introduce the basic structures of the functional architecture. The main idea is that neural computations strictly depend on the organization and connectivity of neurons in the cortex. We will consider only the structures that are relevant to the Sub-Riemannian model presented in the second part of the Chapter, those involved in the boundary coding. There are several mathematical models dealing with visual cortex due to Hoffmann [16], Petitot and Tondut [23], but here we will simply give a presentation of the model of Citti-Sarti [6]. The main goal is to underline how the sub-Riemannian geometry is a natural instrument for the description of the visual cortex.

2.1 The visual cortex and the visual pathway

The primary visual cortex is located in the occipital lobe in both cerebral hemispheres and it surrounds and extends into a deep sulcus called the calcarine sulcus. The primary visual cortex, often called V1, is a structure that is essential to the conscious processing of visual stimuli. Its importance to visual perception can be observed in patients with damaged V1, who generally experience disruptions in visual perception that can range from losing specific aspects of vision to complete loss of conscious awareness of visual stimuli. As reported in [17], vision is generated by photoreceptors in the retina, a layer of cells at the back of the eye. The information leaves the eye through the optic nerve, and there is a partial crossing of axons at the optic chiasm. After the chiasm, the axons are called the optic tract. The optic tract wraps around the midbrain to get to the lateral geniculate nucleus (LGN), where all the axons must synapse. From there, the LGN axons fan out through the deep white matter of the brain as the optic radiations, which

will ultimately travel to primary visual cortex, at the back of the brain.

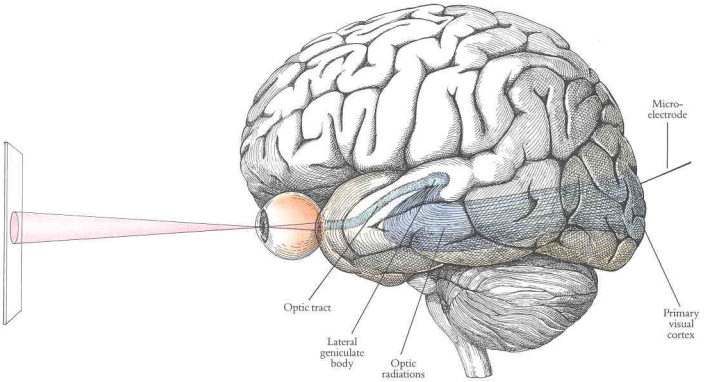

Figure 2.1: The visual cortex and the visual path.

2.2 Simple cells in V1

The primary visual cortex V1 processes the orientation of contours by means of the so called simple cells and other features of the visual signal by means of complex cells (stereoscopic vision, estimation of motion direction, detection of angles). Every cell is characterized by its receptive field, that is the domain of the retinal plane to which the cell is connected with neural synapses of the retinal-geniculate-cortical path. When the domain is stimulated by a visual signal the cell respond generating spikes. Classically, a receptive field (RF) is decomposed into ON (positive contrast) and OFF (negative contrast) zones according to the type of response to light and dark luminance Dirac stimulations. The area is considered ON if the cell spikes responding to a positive signal and OFF if it spikes responding to a negative signal. There exists, therefore, a receptive profile (RP) of the visual neuron, which models the neural output of the cell in response to a punctual stimulus on the 2D dimensional retinal plane. More precisely, a receptive profile is described by a function $\varphi : D \to \mathbb{R}$, where D is the receptive field which is a subset of the retinal plane.

The simple cells of V1 are sensitive to the boundaries of images and have directional receptive profiles, this is the reason why they are often interpreted as Gabor patches (trigonometric functions modulated by a Gaussian). The Gaussian bell will be denoted:

$$G_\sigma(x,y) = \frac{1}{2\pi\sigma^2} \exp^{-\frac{\tilde{x}^2+\tilde{y}^2}{\sigma^2}}$$

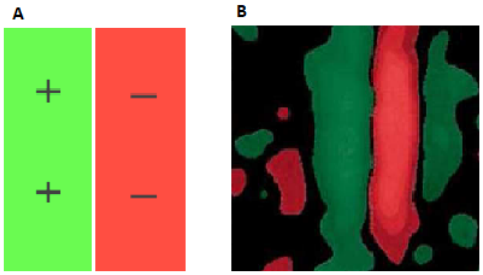

Figure 2.2: Simple cell's receptive profile [6]. A, scheme of the RP structure with regions + (ON) and - (OFF). B, Recordings of the level lines of the RPs.

and the Gabor patch will be:

$$\psi_{\sigma,\omega,\vartheta}(x,y) = \exp^{i\omega\tilde{y}} G_\sigma(x,y) \tag{2.1}$$

where

$$\begin{cases} \tilde{x} = x\cos\vartheta + y\sin\vartheta \\ \tilde{y} = -x\sin\vartheta + y\cos\vartheta, \end{cases} \quad \text{which means} \quad \begin{pmatrix} \tilde{x} \\ \tilde{y} \end{pmatrix} = R_{-\vartheta} \begin{pmatrix} x \\ y \end{pmatrix}, \tag{2.2}$$

for a rotation matrix

$$R_\vartheta = \begin{pmatrix} \cos\vartheta & -\sin\vartheta \\ \sin\vartheta & \cos\vartheta \end{pmatrix}$$

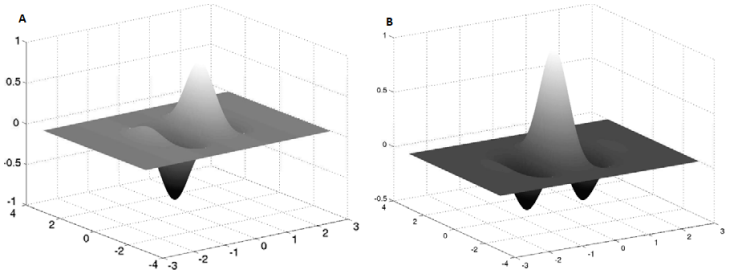

Figure 2.3: A representation of the real (A) and imaginary (B) part a Gabor filter.

Here the angle $\vartheta \in S^1$ describes the orientation of the symmetry axis of the filter, and models the OP of the simple cell. The imaginary part of (2.1) (Figure 2.4 B) models an odd-symmetric RP

$$\varphi_\vartheta(x,y) = \mathrm{Im}(\psi_{\sigma,\omega,\vartheta}) = \frac{1}{2\pi\sigma^2}\sin(\omega\tilde{y})\exp^{-\frac{\tilde{x}^2+\tilde{y}^2}{\sigma^2}}$$

and the real part (Figure 2.4 A) an even one

$$\varphi_\vartheta(x,y) = \mathrm{Real}(\psi_{\sigma,\omega,\vartheta}) = \frac{1}{2\pi\sigma^2}\cos(\omega\tilde{y})\exp^{-\frac{\tilde{x}^2+\tilde{y}^2}{\sigma^2}}.$$

The way in which visual neurons act on the visual stimulus is very complex and includes non trivial temporal dynamics, non linear responses to light intensity and contextual modulation accounting for non local behaviors. For our purpose we will consider receptive fields acting on the stimulus with linear and local behavior as in the following. Let $I(x, y)$ be the optical signal defined on the retina (or equivalently the visual field) and

$$\varphi_{x_0,y_0,\vartheta}(x', y') = \varphi_\vartheta \left(x' - x_0, y - y_0\right) \tag{2.3}$$

be the RP of a neuron defined in a domain D centered on (x_0, y_0). The neuron acts on I as a filter, and it computes the mean value of I on D weighted by $\varphi_{x_0,y_0,\vartheta}$:

$$\mathcal{O}(x_0, y_0, \vartheta) = \int_D I\left(x', y'\right) \varphi_{x_0,y_0,\vartheta}\left(x', y'\right) dx'dy'.$$

The response of the neuron $\mathcal{O}$ can be interpreted as a weighted measure at the point (x_0, y_0) of the signal I. Therefore, if there is a set of neurons with RP φ covering the whole retina, we have:

$$\mathcal{O}(x, y, \vartheta) = \int_D I\left(x', y'\right) \varphi_{x,y,\vartheta}\left(x', y'\right) dx'dy'. \tag{2.4}$$

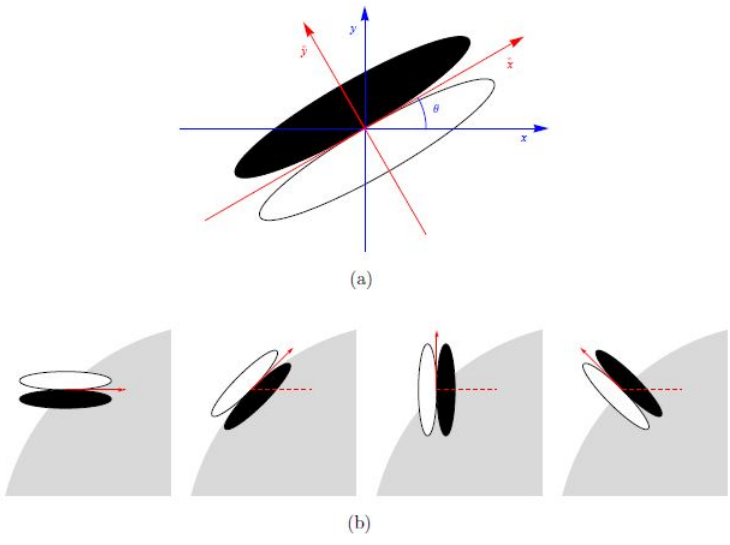

Figure 2.4: A set of simple cells schematically represented in presence of a visual stimulus. This is maximum when the axis (red arrow) is tangent to the boundary, but it is also not nulled for a broad set of sub-optimal orientations. Figure taken from [24].

If simple cells are functionally involved in visual processing as orientation detectors it means that their response is a measure of the local orientation

of the stimulus at a certain retinal point. The angle in which the response of the cell is maximal is called the orientation preference (OP) of the neuron. In presence of a boundary in the visual stimulus, the cell fires maximally when its preferred orientation is aligned with the boundary itself. Nevertheless a broad set of cells with suboptimal orientation respond to the stimulus. Then the cortex is equipped with a neural circuitry that is able to sharpen orientation tuning. With this mechanism, called non-maximal suppression, the output of the cells with suboptimal orientation is suppressed, allowing just a small set of cells optimally oriented to code for boundary orientation.

To understand the image processing operated by the simple cells in V1, it is necessary to consider the functional structures of the primary visual cortex: the *retinotopic organization*, the *hypercolumnar structure* with *intracortical circuitry* and the *connectivity structure* between hypercolumns.

2.3 The functional architecture of the visual cortex

In this section we mostly refer to [4], [7], [16], [17], [18], [22] and [23].

2.3.1 The retinotopic structure

The retinotopic structure is a mapping between the retina and the primary visual cortex that preserves the retinal topology and it is mathematically described by a logarithmic conformal mapping. From the image processing point of view, the retinotopic mapping introduces a simple deformation of the stimulus image that will be neglected in the present study. In this way, if we identify the retinal structure with a plane R and by M the cortical layer, the retinotopy is then described by a map $q : R \to M$ which is an isomorphism. Hence we will identify the two planes, and call M both of them.

2.3.2 The hypercolumnar structure

The hypercolumnar structure organizes the cortical cells in columns corresponding to parameters like orientation, ocular dominance, color etc. For the simple cells (sensitive to orientation) columnar structure means that to every retinal position is associated a set of cells (hypercolumn) sensitive to all the possible orientations. In Figure 2.5 it is shown a simplified version of the classical Hubel and Wiesel [18] cube scheme of the primary visual cortex. Cells belonging to the same column share similar RP characteristics (almost identical receptive fields, same OP and ocular dominance). The orientation hypercolumns are arranged tangentially to the cortical sheet. Moving across the cortex the OP varies while the RP strongly overlap. Oriented

bars colored with a polar color codes are used to represent the OPs (the hue represent the angle).

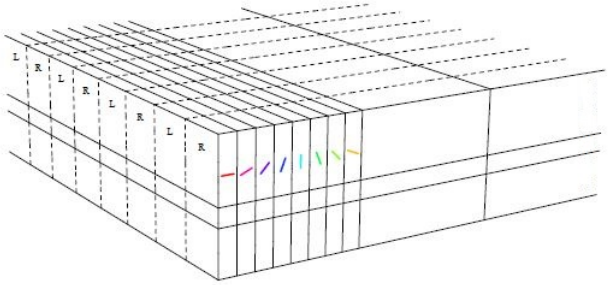

Figure 2.5: Hubel and Wiesel's "ice cube" model of visual cortical processing [18].

We observe that in this first model of the hypercolumnar structure there are three parameters: the position in the retinal plane, which is two dimensional, and the orientation preference of cells in the plane. The visual cortex is however two-dimensional and then the third dimension collapses onto the plane giving rise to the fascinating pinwheels configuration observed by William Bosking [4] with optical imaging techniques. In Figures 2.6 the orientation preference of cells is coded by colors and every hypercolumn is represented by a pinwheel.

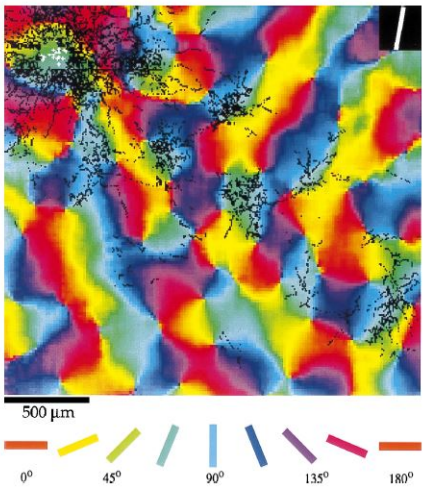

Figure 2.6: A marker is injected in the cortex, in a specific point, and it diffuses mainly in regions with the same orientation as the point of injection (marked with the same color in Figure). Image taken from [4].

As proposed by Hoffmann and Petitot [16], the mathematical structure ideally modelling the hypercolumnar structure is a fiber bundle. As we have seen in the previous Chapter, a fiber bundle is defined by two differentiable

manifolds M and E, a group G with a topological structure, and a projection π. M and E are called, respectively, the base space and the total space of the fiber bundle. Moreover, the total space is locally described as a cartesian product $E = M \times F$, meaning that to every point $m \in M$ is associated a whole copy of the group G, called the fiber. The function π is a surjective continuous map which locally acts as:

$$\pi : M \times G \to M, \quad \pi(m, g) = m,$$

where g is an element of G. In this case, the base space is implemented in the retinal space and the total space in the cortical space. Furthermore, there is a map associating to each retinotopic position a fiber which is a copy of the whole possible set of angular coefficients in the plane $\{\vartheta \in S^1\}$. Therefore, in this case the group G of rotations to the point $m = (x, y) \in M$ is implemented in an hypercolumn over the same point. In this way the visual cortex is modelled as a set of hypercolumns in which over each retinal point (x, y) there is a set of cells coding for the set of orientations $\{\vartheta \in S^1\}$ and generating the 3D space $\mathbb{R}^2 \times S^1$.

In the model of Citti-Sarti the cortex we will described as a differential structure, using the principal fiber bundle of the group of rigid transformations in 2D space ($SE(2)$) as mathematical structure describing the primary visual cortex: we will focus on it in the next sections.

2.3.3 The neural circuitry

The neural circuitry of the primary visual cortex are of two types: the intracortical circuitry and the connectivity structure.

The *intracortical circuitry* is able to select the orientation of maximum output of the hypercolumn in response to a visual stimulus and to suppress all the others. The mechanism able to produce this selection is called *non-maximal suppression* or orientation selection, and its deep functioning is still controversial, even if many models have been proposed. This maximal selectivity is the simplest mechanism to accomplish the selection among all different cell responses to effect a lift in the space of features. Given a visual input I, the neural processing associates to each point (x, y) of the retina M a point $\left(x, y, \bar{\vartheta}\right)$ in the cortex. We interpret this mechanism as a lifting into the fiber of the parameter space $\mathbb{R}^2(x, y) \times S^1(\vartheta)$ over (x, y). Precisely, the odd part of the filters lifts the boundaries of the image and the even part of the filters lifts the interior of the objects. We will denote as $\bar{\vartheta}$ the point of maximal response:

$$\mathcal{O}\left(x, y, \bar{\vartheta}\right) = \max_{\vartheta} \mathcal{O}(x, y, \vartheta). \tag{2.5}$$

This maximality condition can be mathematically expressed requiring that the partial derivative of $\mathcal{O}$ with respect to the variable ϑ vanishes at the point $\left(x, y, \bar{\vartheta}\right)$:

$$\partial_{\vartheta} \mathcal{O}\left(x, y, \bar{\vartheta}\right) = 0.$$

We will also require that at the maximum point the Hessian is strictly negatively definite: $\mathrm{Hess}\,(\mathcal{O}) < 0$.

The *connectivity structure*, also called horizontal or cortico-cortical connectivity is the structure of the visual cortex which ensures connectivity between hypercolumns. The horizontal connections connect cells with the same orientation belonging to different hypercolumns. Recently techniques of optical imaging allowed a large-scale observation of neural signal propagation via cortico-cortical connectivity. These tests have shown that the propagation is highly anisotropic and almost collinear to the preferred orientation of the cell (as in Figure 2.6). It is already confirmed that this connectivity allows the integration process, that is at the base of the formation of regular and illusory contours and of subjective surfaces. Obviously the functional architecture of the visual cortex is much richer that what we have delineated, just think to the high percentage of feedback connectivity from superior cortical areas, but in this paper we will show a model of low level vision, aiming to mathematically model correctly the functional structures we have described.

2.4 A Sub-Riemannian model in the rototranslation group

The Rototranslation group is a fundamental mathematical structure used in the model of Citti-Sarti. In the literature it is also known as the 2D Euclidean motion group $SE\,(2)$. It is the 3D group of rigid motions in the plane or equivalently the group of elements invariant to rotations and translations. The aim of this section is to show that the visual cortex at a certain level is naturally modelled as the Rototranslation group with a sub-Riemannian metric. This section mostly refers to [3], [24], [25] and [26].

2.4.1 The group law

In previous sections we anticipated that the model of Citti-Sarti is a principal fiber bundle of the group of rigid transformations, so let's introduce the group law. It has been observed experimentally that the set of simple cells RPs is obtained via translations and rotations from a unique profile, of Gabor type. This means that there exists a mother profile φ_0 from which all the observed profiles can be deduced by rigid transformation. More precisely, as noted in (2.3), every possible receptive profile is obtained from a mother kernel by translating it of the vector (x_1, y_1) and rotating over itself by an angle ϑ. Therefore, another way of thinking with regards to the functional architecture of the visual cortex is illustrated in Figure 2.7 where the half-white/half-black circles represent oriented receptive profiles of odd simple cells and the angle of the axis is the angle of tuning.

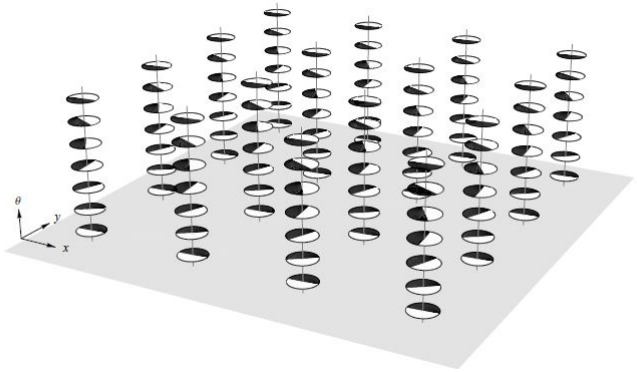

Figure 2.7: The visual cortex modelled as the group invariant under translations and rotations. Figure taken from [24].

We denote $T_{(x_1,y_1)}$ the translation of the vector (x_1, y_1) and R_ϑ a rotation matrix of angle ϑ, defined in (2.2). Then a general element of the $SE(2)$ group is of the form $A_{(x_1,y_1,\vartheta)} = T_{(x_1,y_1)} \circ R_\vartheta$ and applied to a point (x, y) it yields:

$$A_{(x_1,y_1,\vartheta_1)} \begin{pmatrix} x \\ y \end{pmatrix} = \begin{pmatrix} x \\ y \end{pmatrix} + R_{\vartheta_1} \begin{pmatrix} x_1 \\ y_1 \end{pmatrix}.$$

In this way all the profiles can be interpreted as: $\varphi(x_1, y_1, \vartheta_1) = \varphi_0 \circ A_{(x_1,y_1,\vartheta_1)}$. The set of parameters $g_1 = (x_1, y_1, \vartheta_1)$ form a group with the operation induced by the composition $A_{(x_1,y_1,\vartheta_1)} \circ A_{(x_2,y_2,\vartheta_2)}$:

$$A_{(x_1,y_1,\vartheta_1)} \circ A_{(x_2,y_2,\vartheta_2)} = A_{(x_3,y_3,\vartheta_3)},$$

where

$$\begin{aligned} \vartheta_3 &= \vartheta_1 + \vartheta_2 \\ \begin{pmatrix} x_3 \\ y_3 \end{pmatrix} &= R_{\vartheta_1} \begin{pmatrix} x_2 \\ y_2 \end{pmatrix} + \begin{pmatrix} x_1 \\ y_1 \end{pmatrix}. \end{aligned}$$

This turns out to be:

$$g_1 \cdot_{rt} g_2 = (x_1, y_1, \vartheta_1) \cdot_{rt} (x_2, y_2, \vartheta_2) = \left(\left(\begin{pmatrix} x_1 \\ y_1 \end{pmatrix} + \quad R_{\vartheta_1} \begin{pmatrix} x_2 \\ y_2 \end{pmatrix} \right)^T, \quad \vartheta_1 + \vartheta_2 \right).$$

Being induced by the composition law, one can easily check that $\cdot_{rt}$ verifies the group operation axioms, where the inverse of a point $g_1 = (x_1, y_1, \vartheta_1)$ is induced by the rototranslation $R_{\vartheta_1}^{-1} \circ T_{(x_1,y_1)}^{-1}$ and the identity element is given by the trivial point $e = (0, 0, 0)$.
Then, the group generated by the operation $\cdot_{rt}$ in the space $\mathbb{R}^2 \times S^1$ is

called the *Rototranslation group* or equivalently $SE(2)$. A structured space with the symmetries described above allows for the cortex to be invariant to rotations and translations in the representation of a retinal image: the signals will be identical no matter what their position or orientation in the phenomenological space is.

2.4.2 The differential structure

What distinguish a Lie group from a topological group is the existence of a differential structure. In the case of V1, Citti and Sarti proposed to endow the $\mathbb{R}^2 \times S^1$ with a sub-Riemannian structure. In the standard Euclidean setting, the tangent space to $\mathbb{R}^2 \times S^1$ has dimension 3. They selected a bi-dimensional subset of the tangent space at each point, called the horizontal plane, as a model of the connectivity in V1. In the sequel we describe how to define the horizontal plane.

The cotangent bundle

We recall that linear functions defined on the tangent space at a point (x, y) are called 1-forms, or cotangent vectors. The set of 1-forms at a point (x, y) is denoted $T^*(x, y)$ and (in this case) it is a vector space of dimension 2. Its basis is denoted (dx, dy). This means that a general 1-form can be expressed as

$$\omega = \omega_1 dx + \omega_2 dy.$$

By definition, a form is a function defined on the tangent space, and, being linear the action is formally analogous to a scalar product:

$$\omega(X) = \omega_1 \alpha_1 + \omega_2 \alpha_2, \quad X = \alpha_1 \partial_x + \alpha_2 \partial_y.$$

However this operation is called duality, instead of scalar product, since it acts between different spaces: ω_1, ω_2 are coefficients of a 1-form and α_1, α_2 coefficients of a tangent vector.

As mentioned before, the imaginary part of a Gabor filter with orientation ϑ has the expression:

$$\varphi_\vartheta(x, y) = \frac{1}{2\pi\sigma^2} \sin(\omega\tilde{y}) \exp^{-\frac{\tilde{x}^2+\tilde{y}^2}{\sigma^2}},$$

where $(\tilde{x}, \tilde{y})$ have been defined in (2.2). Then, the function φ_ϑ can be approximated (up to a multiplicative constant) by

$$\frac{\sin(\omega\tilde{y})}{2\pi\omega\sigma^4} \exp^{-\frac{\tilde{x}^2+\tilde{y}^2}{\sigma^2}} \simeq \frac{\tilde{y}}{2\pi\sigma^4} \exp^{-\frac{\tilde{x}^2+\tilde{y}^2}{\sigma^4}} = -\frac{1}{2\pi\sigma^2} \partial_{\tilde{y}} \exp^{-\frac{\tilde{x}^2+\tilde{y}^2}{\sigma^2}} = -(\partial_{\tilde{y}} G_\sigma)(\tilde{x}, \tilde{y}).$$

Since the map $(x, y) \mapsto (\tilde{x}, \tilde{y})$ is a rotation, a derivative in the direction $\tilde{y}$ can be expressed in the original variables (x, y, ϑ) as a directional derivative in the direction of the vector $(-\sin\vartheta, \cos\vartheta)$:

$$\partial_{\tilde{y}} G_\sigma = -\sin\vartheta \partial_x G_\sigma + \cos\vartheta \partial_y G_\sigma = \langle (-\sin\vartheta, \cos\vartheta), \nabla G_\sigma \rangle .$$

This derivative expresses the projection of the gradient in the direction of the vector $X_3 = (-\sin\vartheta, \cos\vartheta)$. We will denote it as

$$X_3 = -\sin\vartheta \partial_x + \cos\vartheta \partial_y .$$

If I represents a real stimulus, an image, the simple cell receptive profile acts as in formula (2.4) on the image I. As a consequence of (2.3), the output can be expressed as

$$\mathcal{O}(x, y, \vartheta) = \int_D I(x', y') \varphi_\vartheta (x - x', y - y') dx' dy'$$

$$= (I * \varphi_\vartheta)(x, y) = (I * X_3 G_\sigma)(x, y) = X_3 (I * G_\sigma)(x, y)$$

If σ is sufficiently small $I * G_\sigma$ simply provides a slightly smoothed approximation of I, so that

$$\mathcal{O}(x, y, \vartheta) \simeq X_3 I(x, y) .$$

Recalling the hypercolumnar structure exposed below, we can say that a hypercolumn is modelled as a fiber of RPs and its action on the image is a fiber of directional derivations for every orientation ϑ (Figure 2.7).

This also implies that the output can be approximated by $\langle (-\sin\vartheta, \cos\vartheta), \nabla I \rangle$. Since the gradient is an element of the tangent plane, the vector $(-\sin\vartheta, \cos\vartheta)$, which acts on it will be considered as an element of the cotangent plane, and represented as 1-form

$$\omega = -\sin\vartheta dx + \cos\vartheta dy .$$

Orientation selectivity and "non-maximal" suppression

The intracortical circuitry is able to filter out all the spurious directions and to strictly keep the direction of maximum response of the simple cells. Since $X_3 I$ is the projection of the gradient in the direction of the vector $(-\sin\vartheta, \cos\vartheta)$ the maximum will be achieved at a value $\bar{\vartheta}$, which is the direction of the gradient. Then the output will be maximum when $(-\sin\vartheta, \cos\vartheta)$ is parallel to ∇I or equivalently when it is perpendicular to a level line of the image I. If we call $\bar{\vartheta}$ the point of maximum, condition (2.5) reduces to

$$\left| X_{3|\bar{\vartheta}} I \right| = \max_\vartheta \left| X_{3|\vartheta} I \right| .$$

Proposition 2.1. *The point of maximum over the fiber is attained at the value $\bar{\vartheta}$ of the orientation of image level lines. In other words, the vector $X_1 = \cos\left(\bar{\vartheta}\right)\partial_x + \sin\left(\bar{\vartheta}\right)\partial_y$ is parallel to the level lines at the point (x, y).*

Indeed at the maximum point $\bar{\vartheta}$ the derivative with respect to ϑ vanishes, and we have

$$0 = \frac{\partial\left(X_3 I\right)}{\partial\vartheta}_{|\bar{\vartheta}} = -X_{1|\bar{\vartheta}} I = -\left\langle X_{1|\bar{\vartheta}}, \nabla I \right\rangle.$$

Horizontal plane

Previously we have identified each Gabor filter with an 1-form on the $\mathbb{R}^2$ plane. This form can be lifted to the cotangent space of $\mathbb{R}^2 \times S^1$ into the 1-form:

$$\omega_3 = -\sin\vartheta dx + \cos\vartheta dy,$$

It is easy to verify that the vector fields

$$X_1 = \cos\vartheta\partial_x + \sin\vartheta\partial_y, \quad X_2 = \partial_\vartheta$$

are orthogonal to X_3, so that they belong to the kernel of ω_3. The kernel of a 1-form is a subset of the tangent plane. For this reason the action of simple cells RPs on the image can be modeled as the selection of tangent vector (to the level lines) by a 1-form. In particular, the vector X_1, which describes the direction of the level lines of the image, belongs to the kernel of the form ω_3.
As a direct consequence of the preceding assertion we can deduce that the lifted curves are tangent to the plane generated by the vectors X_1 and X_2. In the standard Euclidean setting, the tangent space to $\mathbb{R}^2 \times S^1$ has dimension 3 at every point. Here we have selected a section X_3 of the tangent space. This defines also a bi-dimensional subset of the tangent space at every point, orthogonal to $X_3\left(\vartheta\right)$. According to Definition 1.17 this is called the *contact plane* or *horizontal plane* (see Figure 2.8). It can be represented as

$$\pi_{x,y,\vartheta} = \{\alpha_1 X_1 + \alpha_2 X_2 : \ \alpha_1, \alpha_2 \in \mathbb{R}\}.$$

This plane is the kernel of the 1-form

$$\omega_3 = -\sin\vartheta dx + \cos\vartheta dy.$$

The lifting process

We clarify the lifting concept in our space. We still consider a real stimulus, represented as an image I. Thus, if I represents an image, the family of level

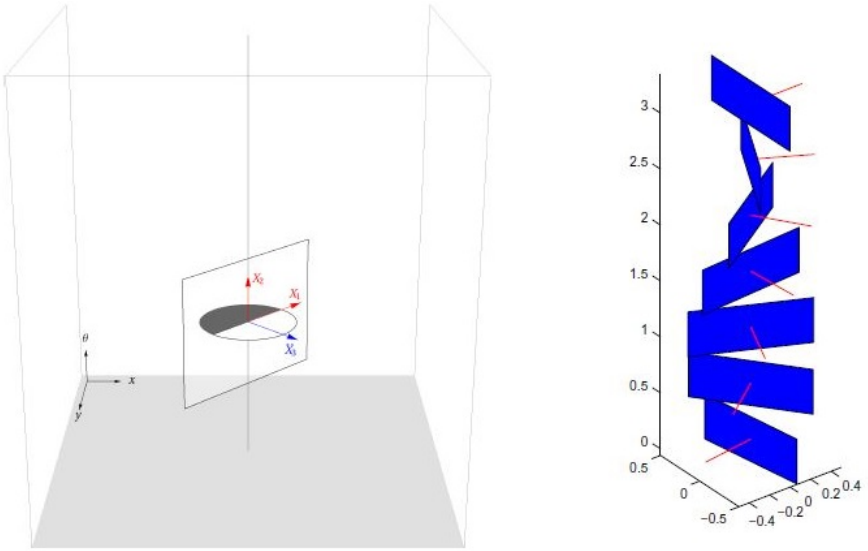

Figure 2.8: A schematic representation of a simple cell of V1 where the vectors X_i are indicated (left) and the contact planes at every point, with the orthogonal vector X_3 (right). Images taken from [24] and [25].

lines is a complete representation of I, from which I can be reconstructed. Hence, a level line may be represented in the 2D plane as a regular curve $\gamma_{2D}(t) = (x(t), y(t))$ and we can assume that its tangent vector is non vanishing almost everywhere, so that for almost every t it can be identified by an orientation $\vartheta(t)$. This indicates that we are able to parametrize the curve by its arc-length

$$(\dot{x}(t), \dot{y}(t)) = (\cos(\vartheta(t)), \sin(\vartheta(t))).$$

The function ϑ takes values on the whole circle, in order to represent polarity of the contours: two contours with the same orientation but with opposite contrasts are represented by opposite angles on the unit circle.
The action of the receptive profiles is to associate to every point $(x(t), y(t))$ the orientation $\vartheta(t)$. Hence the two dimensional curve γ_{2D} is lifted to a new curve $\gamma(t)$ in the 3D space:

$$(x(t), y(t)) \longmapsto (x(t), y(t), \vartheta(t)).$$

We will call *admissible curve* a curve in $\mathbb{R}^2 \times S^1$ if it is the lifting of an edge (identified with a planar curve). Also note that this map defines a function from M to $\mathbb{R}^2 \times S^1$.

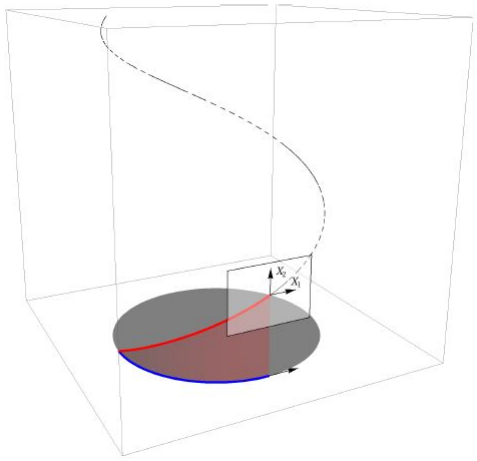

Figure 2.9: A contour represented by the blue curve $\gamma_{2D}(t)$ is lifted into the rototranslation group obtaining the red curve $\gamma(t)$. The tangent space of the rototranslation group is the span of the vectors X_1 and X_2. Figure taken from [24].

Association fields and integral curves

The lifted points of the image would remain decorrelated without an integrative process allowing to connect local tangent vectors and to form integral curves. This process is at the base of both regular contours and illusory contours formation, as written in [23]. The most plausible model of connections is based on a mechanism of "local induction". The specificity of this local induction is described by the association field of Fields, Hayes and Hess experimentally found in [7].

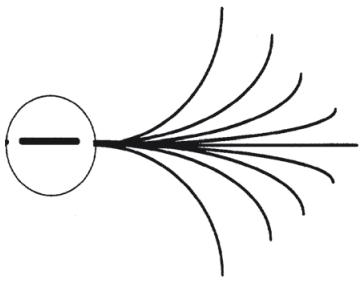

Figure 2.10: Association field from the experiment of Field, Hayes and Hess [7].

The local association field is shown in Figure 2.10 and it can be modeled as a family of integral curves of vector fields belonging to the contact planes spanned by X_1 and X_2, and starting at a fixed point in $\mathbb{R}^2 \times S^1$. Indeed, the lifting of the curve γ_{2D} by definition can be expressed by (x, y, ϑ), where

$$\dot{\gamma}(t) = \left(\dot{x}(t), \dot{y}(t), \dot{\vartheta}(t)\right) = \left(\cos(\vartheta(t)), \sin(\vartheta(t)), \dot{\vartheta}(t)\right) = X_1(t) + \dot{\vartheta} X_2(t).$$

It follows immediately that $\dot{\gamma}(t)$ has a non vanishing component in the direction X_1 and a second component $\dot{\vartheta}$ in the direction of X_2. In particular admissible curves are integral curves of two vector fields in a 3D space, and cannot have components in the orthogonal direction X_3.
As we introduced earlier, the horizontal plane is the span of the vectors X_1, X_2. An admissible curve in this group is an integral curve of the vector field X_1, X_2 and, indicating $\dot{\vartheta}(t)$ as $k(t)$, is defined as the solution for the following ordinary differential equation starting at point (x_0, y_0, ϑ_0):

$$\begin{cases} \dot{\gamma}(t) = X_1(t) + k(t) X_2(t) \\ \gamma(0) = (x_0, y_0, \vartheta_0). \end{cases}$$

Writing the first equation componentwise we get:

$$\begin{cases} \dot{x} = \cos\vartheta \\ \dot{y} = \sin\vartheta \\ \dot{\vartheta} = k(t). \end{cases} \tag{2.6}$$

This parameter k expresses the curvature or angular velocity of the projection of the curve $\gamma(t)$ on the plane (x, y). Writing the curve this way it become obvious that the shape of the curve is completely defined by the function k.

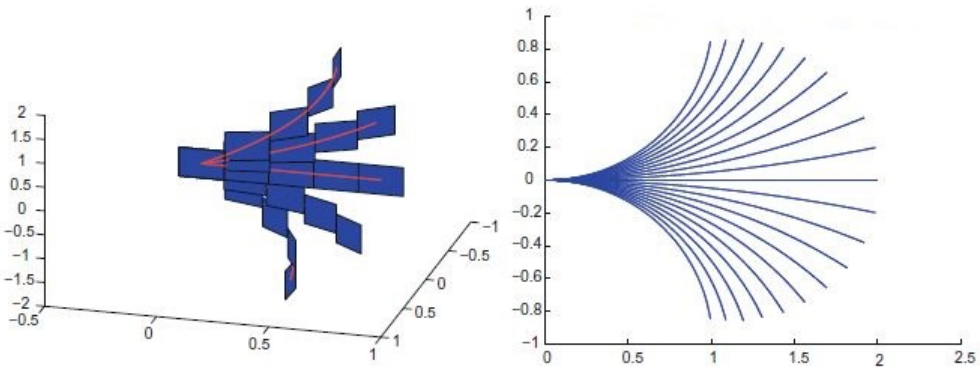

Figure 2.11: Integral curves of the field by varying the parameter k. On the left a 3D representation with contact planes is shown, in the right its projection onto the image plane is visualized. Figure taken from [25].

2.5 Connectivity property and distance

In this section we simply apply the theory set out in the first Chapter to the space chosen by Citti-Sarti [6] to describe the visual cortex.
We explicitly note that the vector fields X_1, X_2 and X_3 are left invariant

with respect to the group law of rotations and translations, so that they are the generators of the associated Lie algebra. We stress the fact that in the standard Euclidean setting, the tangent space to $\mathbb{R}^2 \times S^1$ has dimension three at each point. Here, only a two dimensional section of the tangent space is selected, the horizontal tangent space generated by the vector fields X_1 and X_2.
Hence, we can immediately use Definition 1.9 to define the norm of the vector $\alpha_1 X_1 + \alpha_2 X_2$:

$$\|\alpha_1 X_1 + \alpha_2 X_2\| = \sqrt{\alpha_1^2 + \alpha_2^2}.$$

The metric induced by this choice is clearly Non-Euclidean, moreover it is not even Riemannian at any point, considering we do not prescribe the length of the vector X_3.
Once equipped the horizontal planes with this metric, an admissible curve (represented as in (2.6)) can be computed by integrating the tangent vector, as usual:

$$L(\gamma)(t) = \int_0^t \left|\gamma'(s)\right| ds = \int_0^t \sqrt{1 + k(t)^2} ds.$$

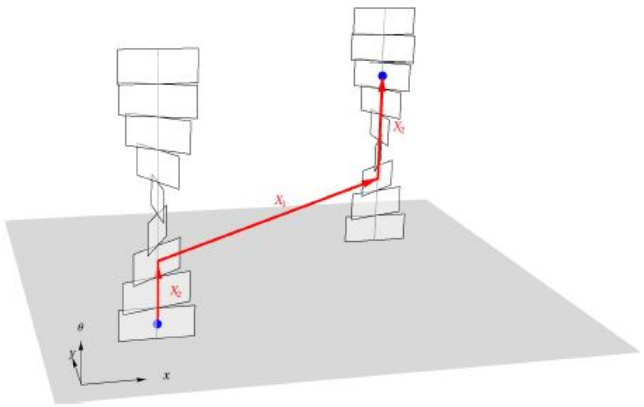

Figure 2.12: A trivial way to reach any point of the $SE(2)$ moving along the integral curves of vectors belonging to the horizontal plane. Figure taken from [24].

In order to define a distance in terms of the length, we need to know if it is possible to connect each couple of points of $\mathbb{R}^2 \times S^1$ using an admissible curve. This is not a simple question taking into account that at each point we have only the directions which are linear combinations of two vectors even if we are immersed in a three dimensional space. Nevertheless we already answered this question in the first Chapter: the possibility of connecting every couple of points with an admissible curve is guaranteed by the Hörmander condition.
In the present case this condition is clearly satisfied since X_1, X_2 and $X_3 =$

$[X_1, X_2] = -\sin\vartheta\partial_x + \cos\vartheta\partial_y$ are linearly indipendent. Hence we can apply the Chow Theorem, which ensures that if the Hörmander condition is satisfied, then the connectivity condition also holds.
Consequently, it is possible to define a notion of distance between two points $p_0 = (x_0, y_0, \vartheta_0)$ and $p_1 = (x_1, y_1, \vartheta_1)$:

$$d(p_0, p_1) = \inf\{L(\gamma) : \gamma \text{ is an admissible curve connecting } p_0 \text{ and } p_1\}.$$

In the Euclidean case this infimum is realized by a geodesic that is a segment. Here, the geodesics are locally curvilinear.

The brain has a modular structure and its parts, also called areas, have comparable structures. So we can assume that the motor cortex structure is similar to the visual cortex one. Now our aim is to find in the motor cortex the same structural aspects of the cells, as the hypercolumnar structure and more generally the functional architecture of the motor cortex, generalizing the structure of the visual cortex above exposed.

Chapter 3

The motor cortex

3.1 The anatomy of movement

The primary motor cortex, or M1, is one of the principal brain areas involved in motor function. M1 is located in the frontal lobe of the brain, along a bump called the precentral gyrus. The role of the primary motor cortex is to generate neural impulses that control the execution of movement. Signals from M1 cross the body's midline to activate skeletal muscles on the opposite side of the body, meaning that the left hemisphere of the brain controls the right side of the body, and the right hemisphere controls the left side of the body.
Other regions of the cortex involved in motor function are called the secondary motor cortices. These regions include the posterior parietal cortex, the premotor cortex, and the supplementary motor area (SMA). The posterior parietal cortex is involved in transforming visual information into motor commands. For example, the posterior parietal cortex would be involved in determining how to steer the arm to a glass of water based on where the glass is located in space. The posterior parietal areas send this information on to the premotor cortex and the supplementary motor area. The premotor cortex lies just in front of the primary motor cortex. It is involved in the sensory guidance of movement, and controls the more proximal muscles and trunk muscles of the body. In our example, the premotor cortex would help to orient the body before reaching for the glass of water. The supplementary motor area lies above, or medial to, the premotor area, also in front of the primary motor cortex. It is involved in the planning of complex movements and in coordinating two-handed movements. The supplementary motor area and the premotor regions both send information to the primary motor cortex as well as to brainstem motor regions.
Neurons in M1, SMA and premotor cortex give rise to the fibers of the corticospinal tract. The corticospinal tract is the only direct pathway from the cortex to the spine and is composed of over a million fibers. These fibers

descend through the brainstem where the majority of them cross over to the opposite side of the body. After crossing, the fibers continue to descend through the spine, terminating at the appropriate spinal levels. The corticospinal tract is the main pathway for control of voluntary movement in humans. There are other motor pathways which originate from subcortical groups of motor neurons (nuclei). These pathways control posture and balance, coarse movements of the proximal muscles, and coordinate head, neck and eye movements in response to visual targets. Subcortical pathways can modify voluntary movement through interneuronal circuits in the spine and through projections to cortical motor regions.

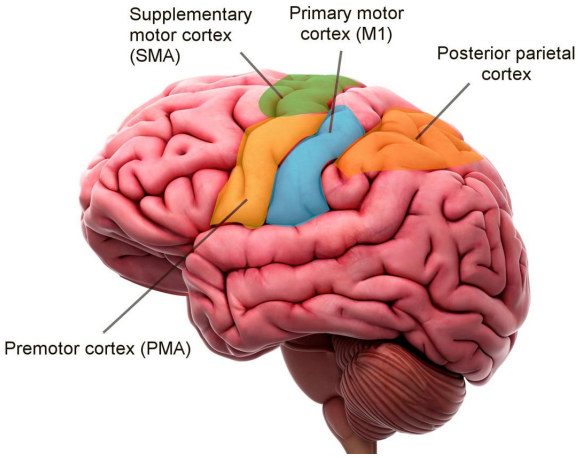

Figure 3.1: Principal cortical domains of the motor system.

3.2 Motor cortical cells activity

The importance of the motor cortex for voluntary limb movements in the primate is well established, nevertheless, the mechanisms by which this function is carried out are not well understood.
In 1978, A. Georgopoulos [9] made the key observation about the direction of arm movement in space as the important variable for cell activity: he settled an experimental apparatus (Figure 3.3) whose purpose was for a monkey to make movements of the same amplitude whose direction would be equally (isotropically) distributed in 2D space. Naturally, this suggested center-out movements, starting from the center of the tablet and ending at the circumference. The results of this experiment were stunning: the activity of single cells in the motor cortex varied in an orderly fashion with the direction of movement in 2D space, cell after cell. Scatterplots of that orderly variation established the *directional tuning curve*.

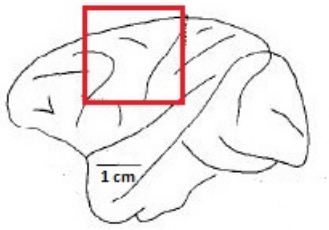

Figure 3.2: Lateral view of the macaque cerebral hemisphere [12]. The area outlined is the region containing cells related to upper proximal arm movements.

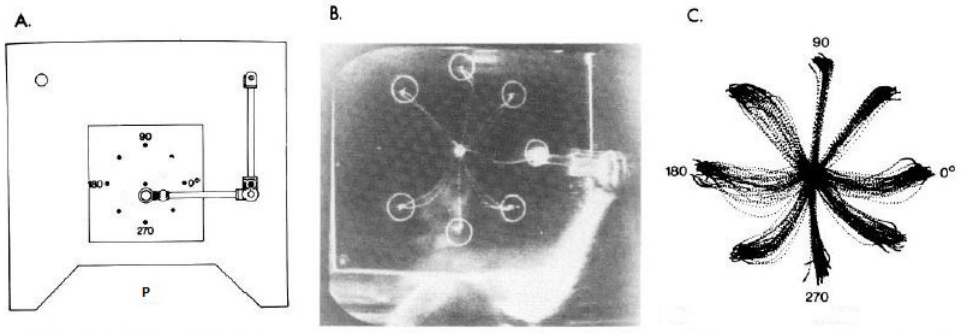

Figure 3.3: *A*, Diagram of the behavioral apparatus [12]. The monkey sits at *position P*, facing a 25-cm square working surface on which there are nine light-emitting diodes (LEDs). One LED is at the center of the working surface and eight are on a circle with an 8-cm radius; they are numbered from 0 to 315 degrees counterclockwise. The monkey grasps an articulated manipulandum at its end and moves it across the (x, y) surface of the plane to capture within a clear plastic circle whichever LED is illuminated. *B*, Overhead view of a monkey performing the task displayed on a television monitor. The monkey has moved the manipulandum from the center to the target LED (in this case, the movement direction is 0 degrees) to complete a trial. The trajectories of movement for this trial and for a few previous trials are superimposed on the television image as light lines. The small circles are the 25-mm-diameter target windows around each target LED. *C*, Trajectories of 30 movements to each target made by a well trained monkey. Each dot is the position of the center of the target-capturing circle on the end of the manipulandum taken at 10-msec intervals.

More specifically, the frequency of discharge of 241 of the 323 cells studied (74.6%) varied in an orderly fashion with the direction of movement; furthermore, these cells ("directionally tuned cells") discharged at higher frequencies to one movement direction, called preferred direction (PD), and at lower rates to other directions.
This resulted in a bellshaped directional tuning curve. In many cells, tuning curves were sinusoidal functions of the direction of movement, that is, the frequency of discharge, D, varied sinusoidally with the angle, ϑ, of the direction of movement, according to the following equation

$$D = b + k \cos\left(\vartheta - \bar{\vartheta}\right), \tag{3.1}$$

where $\bar{\vartheta}$ is the preferred direction and b and k are regression coefficients revealed by statistical analysis. The variable ϑ is the angle formed between the LED situated at the center of the working surface to a particular target. The same conclusion and the same equation occur studying the relations between the neuronal activity in primate motor cortex and the direction of arm movement in three-dimensional (3D) space.

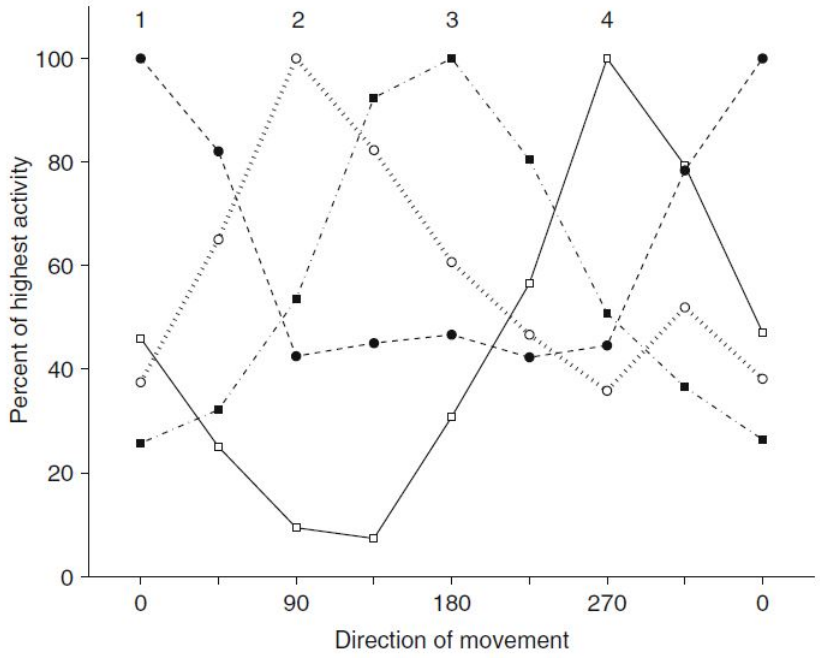

Figure 3.4: Four directional tuning curves, normalized to their maximum, to illustrate the range of the preferred direction across the 360 deg direction 2D space [9].

3.3 Columnar organization of the motor cortex

The discovery by Vernon B. Mountcastle [21] of the columnar organization of the cerebral cortex was the most important discovery of the twentieth century in cortical physiology. Not only did it serve as the framework for the orderly arrangement of knowledge concerning cortical organization and function, but also as a framework for exploring and investigating new ideas and for revisiting old ones about the organization of particular cortical areas.
Following this trail, A. Georgopoulos proposed an idea about the organization (see for example [9], [13], [14]) of the motor cortex and discussed the evidence that the direction of movement was the principle governing motor cortical organization.
His approach was to note the location of cells with specific PD along histologically identified penetrations and then observe possible *en block* changes in PD in penetrations at an angle with anatomical cortical columns.
The results provided strong evidence for a columnar organization of the PD: in penetrations at the exposed cortex, PDs stayed very similar, whereas they changed en block in penetrations at an angle with the anatomical columns. Next step consists on understanding how these columns are organized in the motor cortex.

3.3.1 Mapping of the preferred direction in the motor cortex

Directional tuning is a basic functional property of cell activity in the motor cortex. We have seen that cells with similar preferred directions are organized in columns perpendicular to the cortical surface. Here it is shown how these columns are organized in the tangential dimension on the cortical surface.
The directional tuning of motor cortical cell activity was first described for arm movements in 2D space [12], followed by a generalization for free reaching movements in 3D space [13], [27]. Although the results of studies using 2D armmovements are suggestive, they cannot forma solid basis for a rigorous investigation of the issue of the mapping of the preferred direction because a particular PD in 2D can come from a large number of preferred directions in 3D, with an elevation angle ranging from 0° to 180°. This consideration, and the fact that natural arm movements are typically unconstrained in 3D space, necessitates the use of free reaching 3D movements for a proper mapping study.
It was investigated the possible regularity in the representation of the PD as follows: on a given directionally tuned site, a circular grid consisting of 30-μm annuli extending up to 1200 μm from the center was fit. For every annulus, it has been counted the number of sites recorded from and the number of sites with similar directional tuning to the center site. This

process was repeated for every directionally tuned recording site to derive average estimates of the prevalence of similar PDs away from a given one, determined as the fraction of these sites over the total recorded in an annulus. As expected, the total number of recording sites increased with distance away from the center of the grid as the area of the annulus increased. By contrast, the proportion of similarly tuned sites fell with distance.In fact, the fraction (percentage) of similarly tuned sites F_i in annulus i, with respect to the center site, decreased with distance D_i (μm) from the center as a power fit:

$$F_i = 9.6D_i^{-0.201},$$

where F_i is the fraction (percentage) of sites in the i^{th} annulus, which are significantly correlated to the site at the center.
Next, the detrended data were subjected to spectral analysis to check for and identify possible spatial periodicities in the fluctuation of similarly tuned cells. The spectral analysis revealed two striking peaks at periods of 240 and 86 μm and a finer analysis of higher spatial frequencies using a 10-μm annulus revealed additional significant power at periods $\approx$ 30 and 60 μm. These results suggest:

- a width of a minicolumn of 30μm,
- clustering of two to three minicolumns with similar directions,
- a regular repetition of minicolumns with similar directions every 240μm.

A tentative model of the mapping of PDs in the motor cortex is shown in the figures below (3.5 and 3.6), where given PD is represented by filled circles.

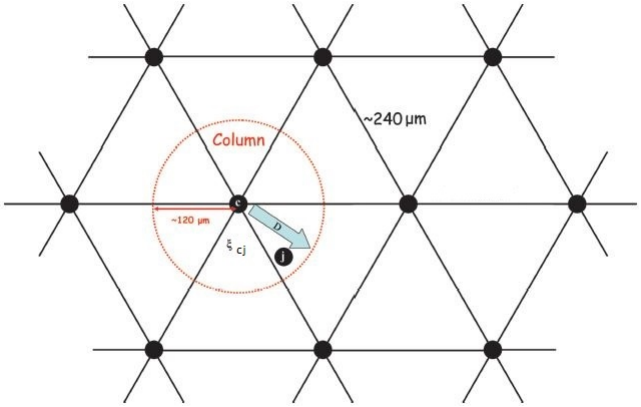

Figure 3.5: Schematic model of mapping of the preferred direction in motor cortex [10]. The quantity ξ_{cj} denotes the angle formed between the PD vector c at the center of the circle and the PD vector j at site j.

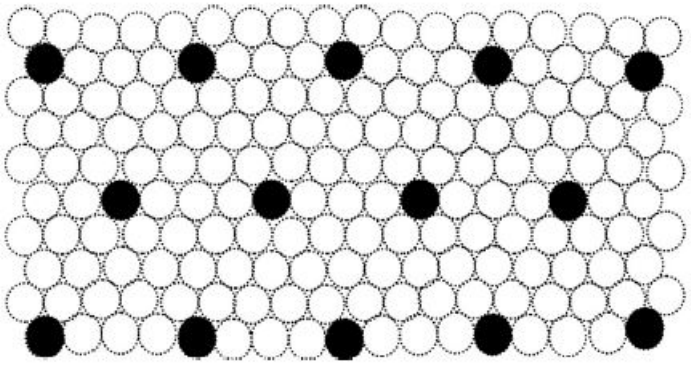

Figure 3.6: Schematic diagram illustrating the periodic pattern of Figure 3.5 in a filled patch of the map [10]. Dimensions (and numbers of columns) are arbitrary.

There are two additional aspects of this model to be considered regarding the PDs within a 240-μm radius circle:

1. there should be wide representations of the PDs;
2. there should be a radial gradient of PDs becoming more and more high from that at the center of the circle, as distance increases away from the center, up to the radius of the circle (120 μm).

The first prediction has been evaluated by examining the distribution of the difference in polar angles (azimuth and elevation) between the one observed at the center of the circle and those observed in a given site within the circle. In accord with the earlier prediction, the angular differences above covered the full range of $-180°$ to $+180°$ for azimuth and $-90°$ to $90°$ for elevation. Then the second prediction has been tested by performing a regression analysis, where the dependent variable was the angle formed between the PD at the center site and the PD at a particular distance from it, and the independent variable was this distance. It has been found a highly statistically significant positive relation for a certain range of distances from 0 to 105 μm to 0 to 120 μm, indicating that the overall angular difference increased with the distance from the center, up to the midwidth of the hypothesized column; this relation disappeared for longer distances. The best fit was an exponential function:

$$\xi_{cj} = 56.6 \exp\left(\frac{D_j}{500}\right),$$
$$D_j \leq 120\mu m,$$

where ξ_{cj} is the angle (°) between the PD at the center and site at distance D_j (μm).
Together these two findings provide evidence for an orderly mapping of the preferred direction in the motor cortex.

3.3.2 First elements for a mathematical structure

We stress the experimental results in which while penetrating the cortex perpendicularly and recording motor cortical cells activity, PDs remain almost constant, no matter the depth. This is a crucial fact because it is the reason why the cortex can be thought of as a 2D layer with respect to movement direction coding. A tangential penetration in the superficial layers of the cortex reveals that cells' activities close to each other strongly overlap while the PDs vary smoothly generating the orientation hypercolumnar structure. In this way, the cortical structure is largely redundant. It means that for each point (x, y) there exists a whole set of neurons in M1 responding maximally to every possible local orientation ϑ (supposing only 2D arm movements). Since ideally the position on the motor cortical layer takes values in the plane $\mathbb{R}^2$ and the preferred direction in the circle S^1, the motor cortex can be locally modelled as the product space $\mathbb{R}^2 \times S^1$. Each point (x, y, ϑ) of this 3D space, represents a column of cells in the cortex associated to a motor cortical layer position (x, y), all of which are tuned to the direction given by the angle ϑ.
Figure 3.7 shows a schematic representation of the motor cortex. The hypercolumns are drawn vertically. The different colors represent different orientations. The coordinates (x, y, ϑ) of this 3D space isomorphic to $\mathbb{R}^2 \times S^1$ are the parameters of motor cortical cells' activity: (x, y) is the motor cortical layer position and ϑ the tuning angle.
The fundamental consideration here is that M1 is modelled as the 3D space of positions and orientations, while as mentioned earlier the cortex is essentially a 2D layer. Therefore, a dimensional reduction problem must be faced: we will see it in the next chapter where we will focus on the mathematical model.

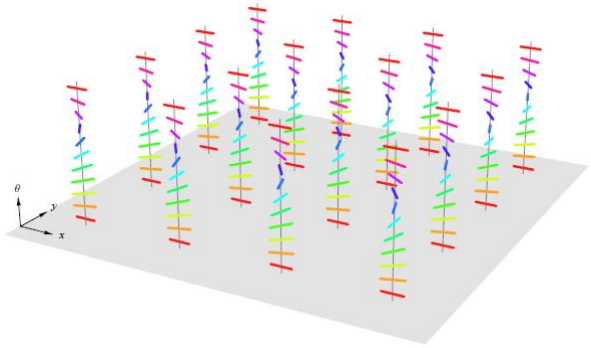

Figure 3.7: The motor cortex modelled as a set of hypercolumns. Over each cortical layer point (x, y) there is a set of cells coding for the set of orientations $\{\vartheta \in S^1\}$ and generating the 3D space $\mathbb{R}^2 \times S^1$. Each bar represents a possible orientation. Figure taken from [24].

There are still many open problems due to this type of structure:

1. how can this structure give rise to movement direction?
2. Until now, we have studied neurophysiological data in which center-out arm movements were performed around the animal's midline and with a fixed center, but what if we change the starting point of the movement?
3. How can motor cortical cells encode movement direction, that is, what is the coordinate system in which an individual cell encodes movement direction?

It is clear that answering these questions will modify the above mentioned structure. We can say we have suggested a structure which suits better this situation: cortical cells have the same Cartesian reference system as the external body space and the movement starting points are restricted to a very small and precise portion of space. Considering this structure as a first attempt at a mathematical model, in the last Chapter we will try to shape a functional architecture able to fit better these above mentioned dynamic and intrinsic aspects of the motor cortex.
Next sections attempt to provide physiological answers to the problems exposed above.

3.4 Coding of the direction of movement

3.4.1 General problem

Studies of single-cell activity have shown that the presentation of a sensory stimulus, or performance in motor tasks, is associated with changes in the discharge of many neurons in each of many brain areas. The question is how a particular function (e.g., judging the quality of a stimulus or planning and executing a movement) is realized by the corresponding neuronal ensemble(s). An indication concerning which aspects of population activity are relevant to a certain function has been provided by careful analysis of the properties of single cells in comparison with the psychophysical capacities of human subjects or animals: can behavioral performance be accounted for by the properties of single cells? If so, no additional principles of population action need to be invoked: in theory, at least, the behavioral capacities in question could be subserved by a neuronal population consisting of functionally homogeneous elements, that is, of cells with the same properties. For example, localization of a stimulus on the body surface, or in the visual field is probably subserved by the activation of cells in the somatic sensory, or visual, areas, respectively, consisting of neurons with receptive fields in the part of the body, or the retina, stimulated. However, in other cases, behavioral capacities cannot be explained on the basis of the functional properties

of single cells, for the relevant information may be available only at the population level. For example, the responses of quickly adapting primary skin afferents carry information concerning the frequency but not the intensity of a vibratory stimulus, although that intensity can be judged very well psychophysically: this suggests that the coding of vibratory intensity is carried by the population of fibers activated.

3.4.2 Neuronal population coding of movement direction

We have seen that individual neurons in the motor cortex of the monkey are broadly tuned with respect to the direction of arm movements toward visual targets in two and three-dimensional space. This suggests that, although single cells possess a preferred direction, many cells will be active for any particular movement and thus that the generation of movement in a particular direction depends upon the activity in the neuronal ensemble. This "population coding" hypothesis has been tested by assuming that contributions from individual neurons add vectorially to yield a neuronal population vector.
Furthermore, a crucial question is whether the population vector calculated from the actual discharge of cells during the reaction time, that is, before the onset of movement, can predict the direction of the upcoming movement. Indeed, this is the case. An example is shown in Figure 3.8, in which the target direction, the time series of the population vector and of the movement are plotted as projections onto the frontal and sagittal planes. It can be seen that the direction of the population vector and of the movement are close to the target direction and that the population vector points in the direction of movement 160 msec before the onset of movement.

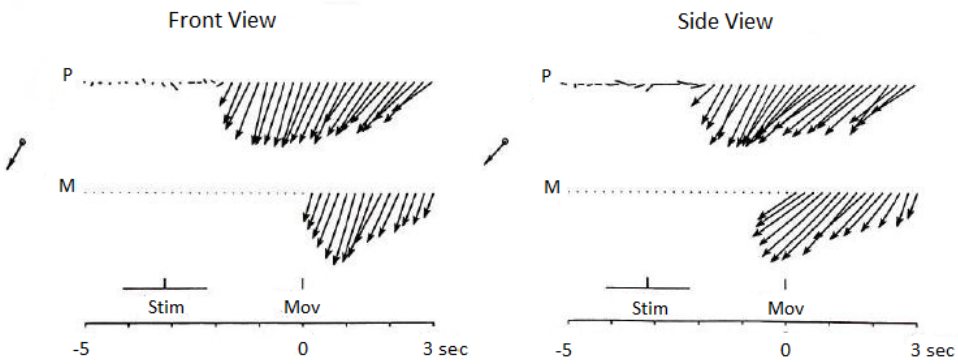

Figure 3.8: Evolution of the population vector in time [11]. Front and side views of time series of population (P) and movement (M) vectors are shown. Population and movement vectors are normalized relative to their respective maximum. Movement vectors are averages from one animal. *Stim*, onset of target light; *Mov*, onset of movement.

The idea used to describe the neuronal population code for a particular movement direction is simple: each cell makes a vectorial contribution ("votes") with direction in the cell's preferred direction and magnitude proportional to the change in the cell's discharge rate associated with the particular direction of movement. The vector sum of these contributions is the outcome of the population code (the *neuronal population vector*) and points in the direction of movement in both 2D or 3D space well before the movement begins.
The results of a statistical analysis used by neurophysiologists (see [11]) showed that the following three conditions are sufficient for the population coding to predict perfectly the direction of movement:

1. the directionally tuned functions must be functions that are radially symmetric around a preferred direction;
2. the preferred directions must be distributed uniformly in 3D (or 2D) space;
3. the values b and k of equation (3.1) must be randomly distributed with respect to the preferred directions.

All neurophysiological data meeet the above requirements [11].

An example of population coding of 3D movement direction is shown in Figure 3.9: the blue lines represent the vectorial contributions of the individual cells when the movement was in the direction indicated by the yellow line. The direction of the population vector is the red line.

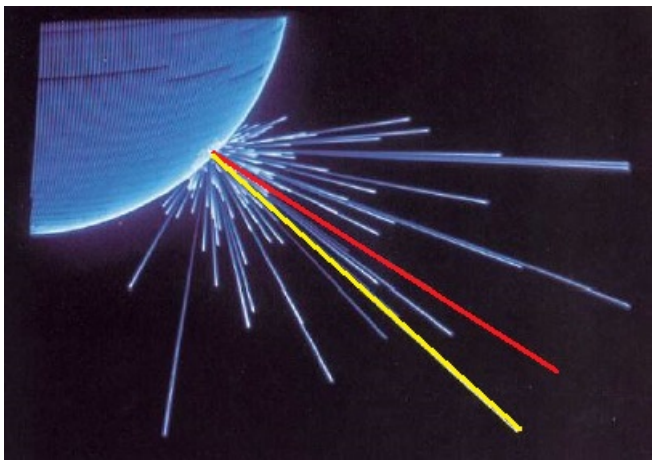

Figure 3.9: An example of population coding of 3D movement direction [11].

Another significant illustration is the following one in which it is repeated the experiment shown in Figure 3.3: each cluster represents the same population and the movement directions are shown in the diagram at the center; even in this case the population vectors (red lines) point approximately in the directions of the movement.

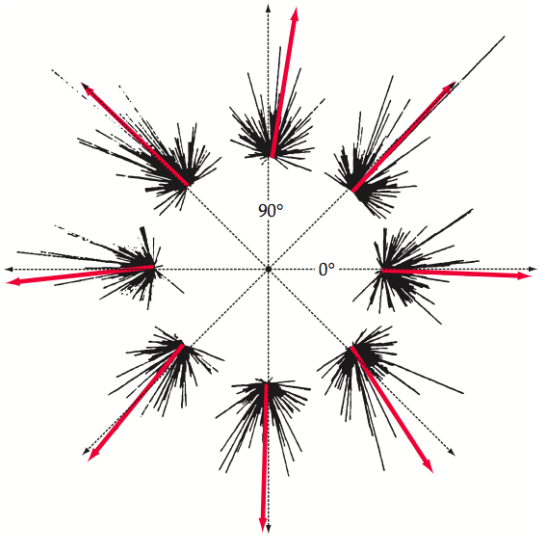

Figure 3.10: An example of population coding of 2D movement directions.

3.5 Arm movements within different part of space: the position dependancy

Until now, we have focused our attention on movements performed only within a single limited region of the work space around the animal's midline. It has been found that, as movements with similar trajectories are made within different part of space, the cells' preferred directions change spatial orientation [5]. This change is of different magnitudes for different cells, but at the level of the population, it follows closely the changes in orientation of the arm necessary to perform the movements required by the task. The task employed in the above experiment was aimed at maintaining similar direction of movement across the work space while changing the underlying patterns of muscular activity and joint angles.

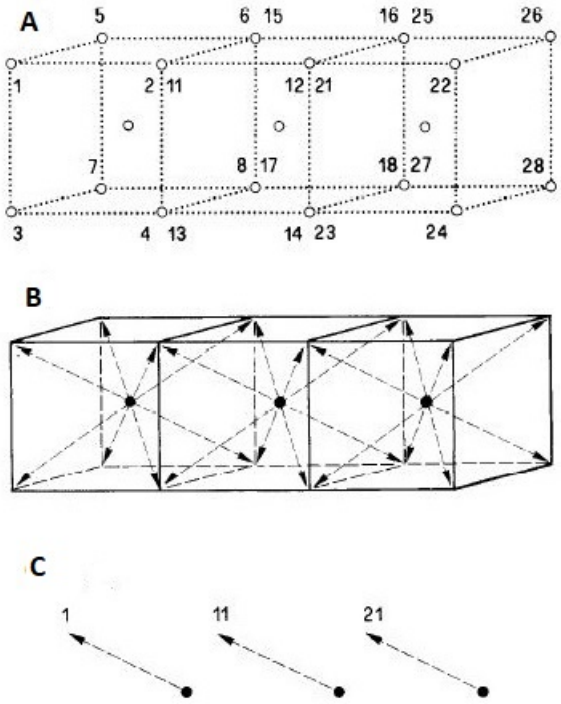

Figure 3.11: *A*, Layout of the workspace pushbottoms (target lights) indicated by open circles [5]. Numbers identify target position in space. Some pushbuttons are labeled by two numbers (2, 11; 12, 21; etc.), indicating that in the task they are targets of movements of two different origins. Numbers also identify the direction of movement. Thus, 2 and 11 identify movements starting from the centers of the left and central parts of the work space, respectively, and directed to target light (2, 11). The animal was seated on a primate chair, 25 cm away from the front lights. The center of the central cube was aligned with the body midline at shoulder height. *B*, Layout of the task showing three sets of movement directions performed in the left, center, and right parts of the work space. Filled circles indicate movement origins within each part of space where monkeys made equal-amplitude (8.7 cm) movements with the same origin in eight different directions (arrows). *C*, 1, 11, 21 indicate one of the eight triplets of movements which traveled along parallel paths in different parts of the work space.

Figure 3.12 shows an example of hand trajectories recorded during the performance of the task. In most instances, the path followed by the hand described a curved trajectory in space. No gross irregularities were observed in these trajectories regardless of where in space the movements were performed. It can be seen that movements made within different parts of the work space travel along paths which are highly similar and in some cases almost parallel.

The main result of this experiment was that, when movements of similar direction were made within different parts of space, the spatial orientation of the preferred directions of motor cortical neurons changed significantly.

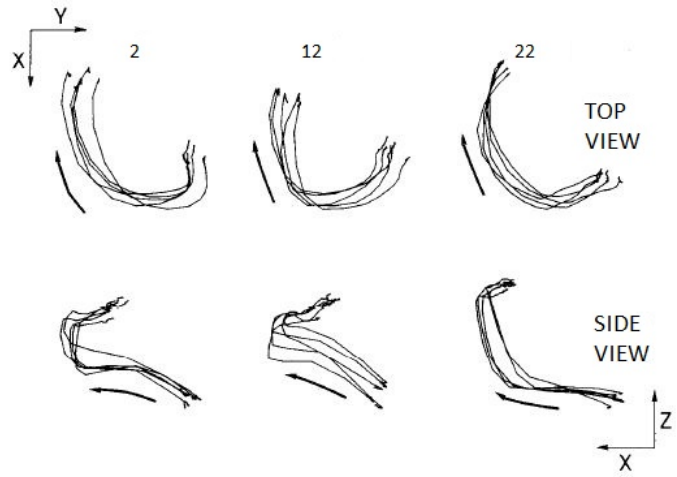

Figure 3.12: Two dimentional plots of top and side views of hand trajectories for movements in directions 2-12-22 [5]. Side views are taken from the right. Five replications are shown for each movement direction. Movements were performed with the left arm.

This modification had a spatial order, following closely the rotation of the shoulder joint in space. Furthermore, it has been revealed that this rotation occurred mainly around the vertical axis but this was most probably due to the behavioral condition imposed by the task which required the animals to make movements within different parts of space separated in the horizontal plane. Indeed, if the animal would have been required to make arm movements in parts of space requiring rotations around a different axis, cell preferred directions would have shown more rotations in other planes. This hypothesis can be experimentally tested. It is interesting that this shift of spatial orientation of cell preferred directions is evident even in the early phase of the reaction time, suggesting that it is the result of a central command.

For 2D arm movements a similar experiment has been done [29]: the whole workspace (including initial position and 8 targets) was translated with respect to the shoulder joint. In this way the arm is a unique entity without considering the elbow and wrist rotations. The vector from the shoulder joint to the initial position (Figure 3.13, black vector) was used as a reference for this transformation. The default workspace had coordinates (0, 0.4) for its initial position, and the vector from the shoulder joint to this initial position was parallel to the positive y-axis. It has been revealed that when the workspace was rotated counter-clockwise by 45° with respect to the shoulder joint (Figure 3.13 *A*, Left), all preferred directions were shifted in the same direction by approximately the same angle (44.83° ± 2.04°) (Figure 3.13 *B*, Left). Similarly, when the workspace was rotated

clockwise by 45° with respect to the shoulder joint (Fig 3.13 *B*, Right), all PDs were shifted in the same direction by approximately the same angle (45.67° ± 3.8°) (Figure 3.13 *B*, Right). Transforming the workspace by 20° clockwise or counterclockwise also shifted the PDs by 20° clockwise or counter-clockwise(not shown). In other words, a shift in the shoulder rotation resulted in a similar shift in the PDs of M1 neurons, which means that the relationship between movement direction and activity of M1 neurons is invariant once the direction is defined relative to the line connecting the shoulder and the initial point of the movement. In summary, rotating the workspace about the shoulder joint shifts all PDs of M1 neurons by the same angle in the same direction.

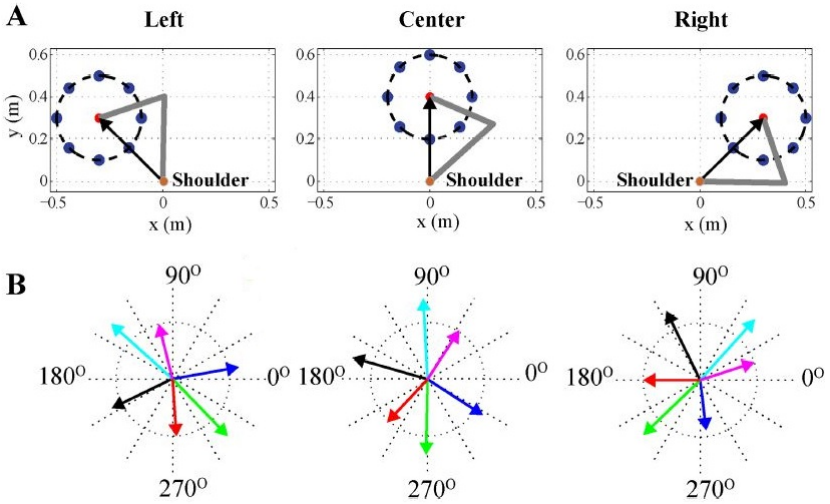

Figure 3.13: Rotating the workspace by an angle shifts the preferred directions in the same direction by the same angle [29]. *A*, Rotation of the workspace about the shoulder. The default workspace (center) was rotated by 45° counter-clockwise (Left), or by 45° clockwise (Right). *B*, The distribution of preferred directions for the three workspaces corresponding to panel A.

Remark 3.1. It should be stressed that the observed invariance between motor cortical cell preferred direction and arm orientation in space was achieved at the population, rather than at the single-cell, level. In the previous section we have seen that the neural population vector is a good predictor of the upcoming movement, however movements have been performed only within a single limited region of the work space, that is around animal's midline. Well, this happens even when the neural population vectors are computed from cell activity recorded in the left and right parts of the work space, thus neural population vector is a good predictor of the upcoming movement regardless of where in space the movement occurs (see [5] and [29]).

Finally, this study suggests another fundamental question: in which coordinate system motor cortical cells encode movement direction? It seems that the motor cortex develops an internal representation of space where the coding of hand trajectory would occur within a coordinate system related, for example, to arm joints angles. We will focus on the coordinates problem in the next Chapter.

Chapter 4

A mathematical model of the motor cortex

In order to shape a mathematical model of the motor cortex we need to clarify the crucial problem of coordinates, namely, we must determine the intrinsic coordinates of the motor cortex.
In this section we refer to [1], [2] and [15].

4.1 The Coordinates problem

Activity in primary motor cortex (M1) has been implicated in a variety of aspects of movement behavior from control of movement execution to participation in movement planning. This means there are correlations between cell firing rates and the following movement variables: hand position, force, hand speed, movement amplitude, target direction, not only movement direction. Nevertheless, we present an analysis focused on cell response components related to a kinematic variable, movement direction, because studies have demonstrated the prevalence and strength of directional coding in M1 and because a large literature exists on center-out tasks in which movement direction is the explicitly controlled variable.
Still, knowing that cell activity strongly reflects a kinematic movement variable like direction does not specify the nature of the cellular representation: Cartesian spatial coordinates, joint angle coordinates, or muscle length coordinates all might be used to represent movement direction at one neural stage or another.
For the entirety of M1, the assumption of a unique coordinate system in which movement direction is encoded may be inappropriate since a heterogeneity of coordinate systems may exist within a single brain region.
Therefore we restrict our analysis to the single-cell level and ask: how can one analyze the coordinate system in which an individual cell encodes movement direction? Beyond outlining a general framework for testing alternative

coordinate hypotheses, we analyze two specific coordinate systems, Cartesian spatial and joint angle.
A key step to investigating alternative coordinate hypotheses is to distinguish between two types of representation of pds: a *spatial pd* and an *internal pd*.

- A *spatial pd* is that hand motion direction, as represented in extrapersonal space, to which a cell will respond maximally during small movements made from a common starting posture. What is meant here by the term "space" is the coordinate system utilized by the experimentalist in making measurements, typically a Cartesian coordinate system whose axes are aligned with the task space: e.g., the planar surface on which the monkey performs a center-out task. This coordinate system will henceforth be referred to as Cartesian spatial coordinates.

- An *internal pd* is that movement direction that elicits maximal cell response when represented in whatever coordinates best characterize the cellular-level encoding of movement direction. This "internal" coordinate system of a cell may be Cartesian spatial coordinates, or it could be some other coordinate system, such as a joint angle or muscle length coordinate system, which is more closely coupled to the biomechanical variables directly affected by the cell through its output connections. Thus, although the spatial pd reflects the internal pd, it is the internal pd that describes a cell's distinctive role in the sensorimotor transformation.

For a well-defined internal coordinate system, mathematical transformations can be used to convert back and forth between a representation of direction in external space and its corresponding representation in the internal space. These transformations are in general posture dependent: the relationship between directions in the internal space and directions in external space changes as a function of posture. By using the distinctions between a spatial pd and an internal pd as well as the posture-dependent properties of the directional transformations between the spaces, a vector field method is developed that generates, for a given cell, spatial pd predictions that differ across the workspace as a function of coordinate hypothesis.

We assume a two joint or two degree of freedom (2-DOF) arm moving on a two dimensional (2D) planar workspace situated within the horizontal plane passing through the shoulder. This model arm, illustrated in Figure 4.1 *A*, will be referred to as the 2-DOF planar arm. A critical feature of the 2-DOF planar arm that simplifies our analysis is that hand position maps uniquely arm posture (which is not the case when the arm possesses redun-

dant degrees of freedom). Thus determining the spatial pd at every posture is equivalent to uniquely determining the spatial pd at every hand position in the workspace. Specifying a spatial direction and a corresponding magnitude over a field of points in space defines a vector field. Thus an internal pd in a particular coordinate system implies a vector field of spatial pds. To illustrate, plots of vector fields of spatial pds were constructed under the assumption of each of two internal coordinate systems for a sample cell whose spatial pd is 60° at a reference posture (see Figure 4.1).

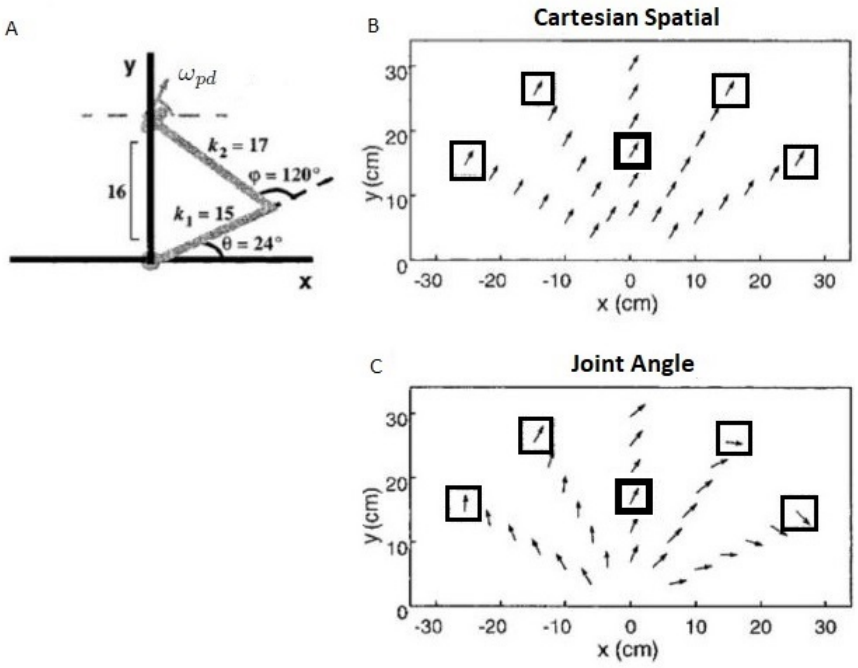

Figure 4.1: *A*, model right arm and spatial preferred direction (pd) at the reference posture. The model describes a 2-link planar arm controlled by shoulder flexion/extension and elbow flexion/extension: k_1 denotes the length of the upper arm segment and k_2 denotes the length of the lower arm segment. A shoulder rotation (denoted by ϑ) of 24° and an elbow rotation (denoted by φ) of 120° specify the reference posture of the arm. At this posture, which places the hand at the point (0,16), the spatial pd of the sample cell is 60°. All lengths are given in cm. *B-C*, vector fields of spatial pds are constructed for the sample cell under the assumption of each of the two internal coordinate systems. For each plot, the vector in the center of the workspace, surrounded by the thick gray box, corresponds to the spatial pd at the reference posture, which, by definition, is identical for the two coordinate hypotheses. The other vectors correspond to spatial pd predictions at differen workspace locations. Using the direct sampling paradigm, one can, on a cell-by-cell basis, compare spatial pd predictions at a small number of other postures (such as those enclosed by the thin gray boxes) to the observed spatial pds to compare the goodness-of-fit of the alternative coordinate systems.

4.1.1 Cartesian spatial coordinates

The simplest vector field arises when the internal coordinate system in which a cell encodes movement direction is the same Cartesian spatial coordinate system in which spatial pds are measured. Spatial pds for this case will not vary with posture because the spatial pd at the reference posture is also the cell's internal pd; in other words, the identity transformation converts between the two representations of direction. Figure 4.1 *B* shows this constant-direction vector field of spatial pds. The magnitude of each vector is unity, indeed for this and subsequent vector field plots, information regarding the direction but not magnitude of the vectors is provided. A vector at a given point in these vector field plots represents the cell's expected spatial pd if the center-out task were performed with that point as the movement origin.

4.1.2 Joint angle coordinates

An M1 cell may encode movement in a joint angle coordinate system that represents a later stage in the sensorimotor transformation from spatial coordinates to muscle activations. Psychophysical studies on motor adaptation have implicated joint-based representations.
The forward and inverse kinematic equations of a 2-DOF planar arm are

$$\begin{cases} x = k_1 \cos(\vartheta) + k_2 \cos(\vartheta + \varphi) \\ y = k_1 \sin(\vartheta) + k_2 \sin(\vartheta + \varphi), \end{cases}$$

$$\begin{cases} \vartheta = \arctan\left(\frac{y}{x}\right) - \arccos\left(\frac{r^2 + k_1^2 + k_2^2}{2k_1 r}\right) \\ \varphi = \arccos\left(\frac{r^2 - k_1^2 - k_2^2}{2k_1 k_2}\right), \end{cases}$$

where $r = \sqrt{x^2 + y^2}$.

Therefore we can roughly assume that the transformation T from the internal coordinate system to the extern is

$$\begin{aligned} T : [0, 2\pi] \times [0, \pi] &\longrightarrow \mathbb{R}^2 \\ (\vartheta, \varphi) &\longmapsto (k_1 \cos(\vartheta) + k_2 \cos(\vartheta + \varphi), k_1 \sin(\vartheta) + k_2 \sin(\vartheta + \varphi)). \end{aligned}$$

The Jacobian matrix is

$$J_T(\vartheta, \varphi) = \begin{pmatrix} -k_1 \sin(\vartheta) - k_2 \sin(\vartheta + \varphi) & -k_2 \sin(\vartheta + \varphi) \\ k_1 \cos(\vartheta) + k_2 \cos(\vartheta + \varphi) & k_2 \cos(\vartheta + \varphi) \end{pmatrix}$$

and the inverse Jacobian is

$$J_T^{-1}(\vartheta, \varphi) = \frac{1}{k_1 k_2 \sin(\varphi)} \begin{pmatrix} k_2 \cos(\vartheta + \varphi) & k_2 \sin(\vartheta + \varphi) \\ -k_1 \cos(\vartheta) - k_2 \cos(\vartheta + \varphi) & -k_1 \sin(\vartheta) - k_2 \sin(\vartheta + \varphi) \end{pmatrix}.$$

Suppose the spatial pd of a cell at a reference posture of (ϑ_R, φ_R) is ω_{pd}. This direction can be recast as a cartesian velocity vector of the form $(\cos(\omega_{pd}), \sin(\omega_{pd}))$, which, when multiplied by $J_T^{-1}(\vartheta_R, \varphi_R)$, yields the internal pd, $\left(\dot{\vartheta_{pd}}, \dot{\varphi_{pd}}\right)^T$, which corresponds to a velocity vector in joint angle space. Let this joint synergy be normalized in joint angle space as $\left(\dot{\vartheta^*_{pd}}, \dot{\varphi^*_{pd}}\right)^T$.
The corresponding vector field of spatial pds is constructed as

$$\begin{pmatrix} v_x(\vartheta, \varphi) \\ v_y(\vartheta, \varphi) \end{pmatrix} = J_T(\vartheta, \varphi) \begin{pmatrix} \dot{\vartheta^*_{pd}} \\ \dot{\varphi^*_{pd}} \end{pmatrix}$$

by letting ϑ and φ vary across their allowable range of values.
We observe that since the Jacobian is posture dependent, application of the inverse Jacobian followed by application of the forward Jacobian evaluated at a new posture is not equivalent to operating with the identity transformation; the composite transformation will result in a new spatial pd.
An intuitive explanation of what it means for a cell to possess an internal pd in a joint angle coordinate system is as follows. Suppose the internal pd for a cell is

$$\begin{pmatrix} \dot{\vartheta_{pd}} \\ \dot{\varphi_{pd}} \end{pmatrix} = \begin{pmatrix} 1 \\ 3 \end{pmatrix},$$

where $\dot{\vartheta_{pd}}$ and $\dot{\varphi_{pd}}$ correspond to the relative shoulder and elbow components of the preferred velocity vector in joint angle space. Such a cell responds maximally to directions of coordinated two-joint motions produced when the elbow rotation rate is three times the shoulder rotation rate. Depending on the posture, the spatial movement direction that corresponds to this movement direction in joint angle space will vary. Figure 4.1 *C* depicts the vector field of spatial pds generated for the sample cell with a constant pd in joint angle coordinates.

4.1.3 Population distributions of preferred directions

Just as the assumption of an internal coordinate system can predict variations in the preferred direction of an individual cell, so too can it predict variations in the distribution of preferred directions over a population of directionally tuned cells. The population level analysis requires a determination of the distribution of preferred directions at a reference posture. In the case of 2-DOF planar arm model neurophysiologists have supposed a roughly uniform distribution of preferred directions at a central posture. They adopted this assumption in their simulations and the vector field approach can analyze distributional variations associated with any distribution that is found at a reference posture.

Under the assumption of Cartesian spatial coordinates, a cell's preferred direction does not change throughout the workspace. When joint angle coordinates are assumed, however, significant alterations in the population distribution will occur since the Jacobian rotates joint angle velocities vectors in a highly non-uniform manner. Figure 4.2 *A* plots the distributions of preferred directions at six workspace locations for a sample population exhibiting a uniform distribution at a central posture. Each distribution is represented by a polar histogram plot. The uniform distribution at the reference posture becomes skewed in a systematic and geometrically sructured manner as a function of workspace location.

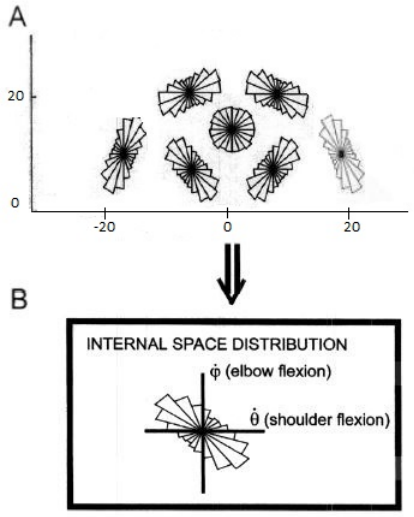

Figure 4.2: Distributions of spatial pds assuming spatial uniformity. *A*, Polar plots of the distributions of spatial pds at six different workspace locations assuming a uniform spatial distribution at a central reference posture. The distributions vary in an orderly and symmetrical fashion that reflects the underlying symmetries of the Jacobian when the upper and lower arm segments are roughly equal in lenght. *B*, The corresponding internal distribution of cells that engenders a uniform distribution at the reference posture. Note the pronounced asymmetry in joint angle space with bias towards the axis that corresponds to opposing motions about the two joints. Motion along that axis could not be induced by cells which activated individual bi-articular muscles since such muscles will induce either flexion or extension about both joints. Instead, if such an internal distribution actually exists, some higher level modularization of the motor periphery would be required to generate a prevalence of joint synergies along the axis indicated.

In generating Figure 4.2 *A*, a uniform distribution of spatial pds at the reference posture is transformed into a distribution of internal pds. This internal distribution, plotted in Figure 4.2 *B* in a coordinate system whose axes correspond to shoulder and elbow rotation rates, will not be uniform because it was generated by application of the inverse Jacobian. A direction

in the coordinate system of Figure 4.2 *B* indicates the relative shoulder and elbow components of the joint synergy to which a cell is tuned.
As the plot shows, the most prevalent joint synergies are those composed of equal parts shoulder extension and elbow flexion or those composed of equal parts shoulder flexion and elbow extention.
Although we assumed a uniform distribution of spatial preferred directions at a reference posture, we could alternatively posit a uniform distribution in the internal space and compute the corresponding spatial distributions. Figure 4.3 *B* shows the spatial pd distributions that result from the assumption of uniformity in the internal space (depicted in Figure 4.3 *A*). We note that the distributions in Figure 4.3 *B* are more highly skewed tham the distributions in Figure 4.2 *A*, moreover even the distribution at the central reference posture demonstrates a strong bias. This fact is interesting because we have seen in the section dedicated to the neuronal population that the direction of movement is considered as a weighted average with weights given by single cells preferred directions. Thus, the distribution of spatial PDs assuming joint angle coordinates in this sense is indicative of movements that are not equally distributed according to the position in which the arm is located.

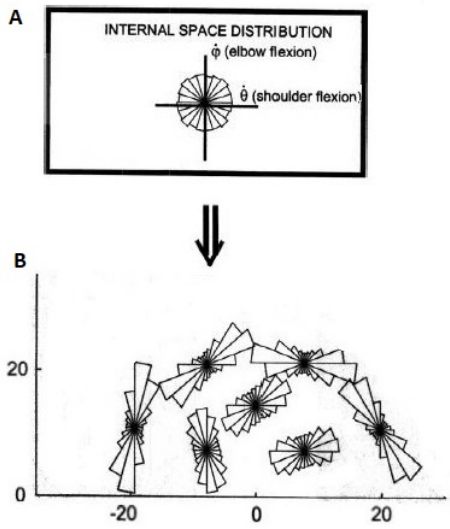

Figure 4.3: Distributions of spatial pds assuming uniformity in joint angle space. *A*, The polar plot of a uniform distribution of pds in jpint angle space. *B*, The spatial pd distributions at the same workspace locations as in Figure 4.2 A when a uniform distribution in the internal space is assumed. These distributions are generally more skewed than their counterpartd in Figure 4.2 A. Even the distribution at the central reference posture demonstrates a strong bias. Ultimately, the spatial pd distributions must be determined empirically, although coordinate analysis can determine whether the variation of distributions across the workspace is consistent with a particular coordinate hypothesis.

Now we have enough information to attempt to shape a mathematical model. First of all we need to translate the motor cortical structure into a mathematical form: is there any instrument capable of describing the columnar organization occured in M1? Yes, there is, we have showed it in the first Chapter and is called *Fiber Bundle*.
The key concept of fiber bundle has been elaborated for deep reasons: how to model processes that require to associate at each point of a base M an entity of certain type F that is regularly depending on this point?

4.2 The structure of motor cortical cells

We study the set of motor cortical cells pointing out that we will distinguish between 2D and 3D arm movements. In the first case, we will refer to movements that range in the body transverse plane (Figure 4.4).

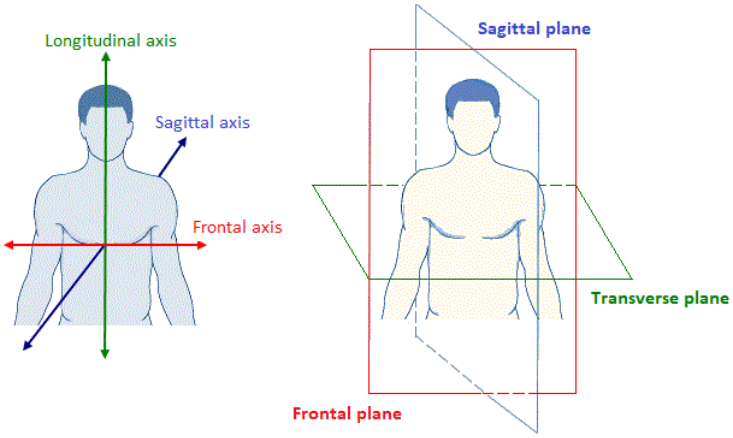

Figure 4.4: Principal axes and planes of movement.

4.2.1 A first "static" model

2D arm movements

In this first approach, we focus on center-out movements of the type discussed in the previous Chapter in section 3.2 with movements relative to the transverse plane of the body rather than to the frontal plane. Moreover, we suppose that movements are restricted to a very *small* portion of the body transverse plane. Since in [2] it is shown how spatial pds do not vary significantly over small arm postural changes under any of the two coordinate systems considered, we assume as coordinate system for motor cortical cells the Cartesian coordinate system.
Since the hypercolumnar structure measured by Georgopoulos in [9] and [10]

organizes the cells of M1 in columns corresponding to movement direction, taking inspiration from visual cortex mathematical models analyzed in the second Chapter, we might suppose that to every position (x, y) is associated a full fibre of possible movement directions.
More specifically, we suppose that a motor cortical cell can be represented by a point (x, y, ϑ) where (x, y) denotes a 2 dimensional position and ϑ denotes cell's PD in position (x, y). We point out that we consider the point (x, y) in a Cartesian reference system centered in the shoulder as represented in Figure 4.1 *A*.

Hence, for this very particular and approximate case, the primary motor cortex structure can be naturally described by a principal fiber bundle (E, M, F, π), where:

- $M \subset \mathbb{R}^2$ represents the hand position in the body transverse plane;
- $F = S^1$ represents movement directions in the plane;
- $E = M \times S^1$ represents the (arm area of the) motor cortex;
- $\pi : M \times S^1 \to M$ is a surjective differential map, which locally acts as follows: $\pi(x, y, \vartheta) = (x, y)$;
- $s : M \to M \times S^1$ represents the selection of a point on a fiber of possible orientations at position $(x, y) \in M$, namely it associates the point (x, y) to a point $\left(x, y, \bar{\vartheta}\right)$.

For simplicity we suppose that the total space E of the principal fiber bundle is $\mathbb{R}^2 \times S^1$.

Remark 4.1. A fundamental dimensional constraint must be taken into account: the total space $E = \mathbb{R}^2 \times S^1$ of the fiber bundle is three-dimensional, whereas as mentioned in the previous Chapter the cortex is essentially a 2D layer; therefore there is a problem of dimensional collapse.
There is the same problem in the visual cortex and in this case the third dimension collapses onto the plane giving rise to the pinwheels configuration. For the motor cortex, pinwheel configuration is suggested from the experiments of Georgopoulos presented in subsection 3.3.1.

Remark 4.2. It is important to recognize what concerns the functional architecture of the motor cortex with motor cortical cells' activity. Indeed, in the geometric structure proposed above, there is a strong redundancy in columns: a point of the fiber bundle actually corresponds to an entire column, which means that each cell has a whole range of choice between all possible movement directions in the plane. Single cell's preferred movement direction does not deal with cortical structure, but cellular activity.

3D arm movements

In this case the approach is the same of the previous one, but this time movement starting points are located in a small region of the body transverse plane and movement directions are restricted on a small region of space.
If we fix the origin of a coordinate system $(O; x, y, z)$ in the spatial point in which the hand is located to start movement, then movement direction in space is identified by two angles ϑ_1 and ϑ_2, called respectively azimuth and polar angle. More precisely, the polar angle ϑ_2 is measured from a fixed zenith direction, parallel to the longitudinal body axis, whereas the azimuth ϑ_1 is measured on a reference plane that passes through the origin and that is parallel to the body transverse plane.
In this way, we suppose that a motor cortical cell can be represented by a point $(x, y, \vartheta_1, \vartheta_2)$ where (x, y) denotes a 2 dimensional position and the couple $(\vartheta_1, \vartheta_2)$ denotes cell's PD in position (x, y).
Thus, as extension of the previous model, we can again describe the primary motor cortex structure as a principal fiber bundle (E, M, F, π), where:

- $M \subset \mathbb{R}^2$ represents hand position in the 3D space;
- $F = S^2$ represents movement directions in the 3D space;
- $E = M \times S^2$ represents the (arm area of the) motor cortex;
- $\pi : M \times S^2 \to M$ is a surjective differential map, which locally acts as follows: $\pi(x, y, \vartheta_1, \vartheta_2) = (x, y)$;
- $s : M \to M \times S^2$ represents the selection of a point on a fiber of possible orientations at position $(x, y) \in M$, namely it associates the point (x, y) to a point $\left(x, y, \bar{\vartheta}_1, \bar{\vartheta}_2\right)$.

Even this time for simplicity we suppose that the total space E of the principal fiber bundle is $\mathbb{R}^2 \times S^2$.

Remark 4.3. Many times in this section has been repeated the "small" adjective to refer to the portion of space in which movements are considered. This is due to what we have seen in the previous Chapter in section 3.5: as movements even with similar trajectories are made within different part of space, cells' preferred directions change spatial orientation. Therefore, in this first mathematical model we have considered a small part of the space in which movement directions may vary as we have not yet really inserted a mathematical tool capable of describing cellular activity dependence on arm position.
Since there are many gaps between mathematical structure and physiological research, clearly the above proposed model cannot be exhaustive, therefore we will propose another approach.

4.2.2 Shoulder joint angle model

2D arm movements

For 2D arm movements we have seen in the previous Chapter that a shift in the shoulder rotation results in a similar shift in the PDs of M1 neurons, which means that the relationship between movement direction and activity of M1 neurons is invariant once the direction is defined relative to the line connecting the shoulder and the initial point of the movement (see [29] for more details). In other words, the difference between arm position, identified by an angle ϑ, and cell's preferred movement direction is constant and represents the movement direction measured from a cell with respect to the position ϑ.
In this way, considering the arm as a unique entity that moves only by spinning the shoulder, we can assume that movement direction is identified by the shoulder rotation angle. Thus, we are supposing that motor cortical cells encode movement direction in joint angle reference system in the simplified case where we do not consider the elbow joint angle.
Following this idea, we hypothesize that over each point $\vartheta \in S^1$ representing arm position, there is a full fibre of possible orientations $\vartheta - \bar{\vartheta}$, where the angle $\bar{\vartheta}$ varies in S^1 and represents motor cortical cell's PD.
Therefore, we propose a principal fiber bundle (E, M, F, π) as a M1 structure, where:

- $M = S^1$ represents arm position in the body transverse plane;
- $F = S^1$ represents all possible movement directions $\vartheta - \bar{\vartheta}$ measured by the cell at position $\vartheta \in M$;
- $E = M \times S^1$ represents the (arm area of the) motor cortex;
- $\pi : M \times S^1 \to M$ is a surjective differential map, which locally acts as follows: $\pi\left(\vartheta, \vartheta - \bar{\vartheta}\right) = \vartheta$;
- $s : M \to M \times S^1$ represents the selection of a point on a fiber of possible movement directions in response to the impulse derived from $\vartheta \in M$.

3D arm movements

Regarding arm movements in space, we know that when movements of similar direction are made within different parts of space, the spatial orientation of the preferred directions of motor cortical neurons changes significantly. Moreover, as in the 2D case, this modification follows closely the rotation of the shoulder joint in space (see [5] for more details). Therefore, even this

time, the difference between arm position and cell's preferred movement direction is constant and represents the movement direction measured from a cell with respect to the position $(\vartheta_1, \vartheta_2)$.
Indeed, due to 3D space, arm position and cell's preferred movement direction are identified by two angles each, the azimuth and polar angle.
In this way, keeping the hypothesis that arm is a unique entity moving only by spinning the shoulder, we can assume that movement direction is identified by the shoulder rotation angle. Then, we hypothesize that over each point $(\vartheta_1, \vartheta_2)$, representing arm position, there is a full fibre of possible orientations $\left(\vartheta_1 - \bar{\vartheta_1}, \vartheta_2 - \bar{\vartheta_2}\right)$, with $\left(\bar{\vartheta_2}, \bar{\vartheta_2}\right)$ varying in S^2 and representing motor cortical cell's PD in space.
Thus, as extension of the previous model, we propose a principal fiber bundle (E, M, F, π) as a M1 structure, where:

- $M = S^2$ represents arm position in space;
- $F = S^2$ represents all possible movement directions $\left(\vartheta_1 - \bar{\vartheta_1}, \vartheta_2 - \bar{\vartheta_2}\right)$ measured by the cell at position $(\vartheta_1, \vartheta_2) \in M$;
- $E = M \times S^2$ represents the (arm area of the) motor cortex;
- $\pi : M \times S^2 \to M$ is a surjective differential map, which locally acts as follows: $\pi\left(\vartheta_1, \vartheta_2; \vartheta_1 - \bar{\vartheta_1}, \vartheta_2 - \bar{\vartheta_2}\right) = (\vartheta_1, \vartheta_2)$;
- $s : M \to M \times S^2$ represents the selection of a point on a fiber of possible movement directions in response to the impulse derived from $(\vartheta_1, \vartheta_2) \in M$.

4.2.3 Shoulder and elbow joint angle model

We show a model which is also be inspired by [28] and it is limited to 2D arm movements.

2D arm movements

Now we want to submit a 2D model which has as internal coordinate system for motor cortical cells the joint angle coordinates previously exposed.
In this way, arm position in the body transverse plane is identified by two angles ϑ and φ representing respectively the shoulder and elbow arrangement in the plane, as shown in Figure 4.1 *A*. Using the same ideas developed in the previous models and the neurophysiological data achieved in [5] and [29], we can reasonably suppose that a shift in the shoulder and elbow rotation results in a similar shift in the PDs of M1 neurons. In this way, another time the difference between arm position, identified by the angles ϑ and φ, and motor neurons preferred movement direction is constant, pointing out that

this difference represents the movement direction measured from a motor cortical cell with respect to the position (ϑ, φ). Therefore, we are assuming as movement direction the shoulder and elbow rotation angles relative to the arm arrangement in the plane. We then hypothesize that over each point (ϑ, φ), representing arm position, there is a full fibre of possible movement directions $\left(\vartheta - \bar{\vartheta}; \varphi - \bar{\varphi}\right)$, where the angle $\bar{\vartheta}$ varies S^1, the angle $\bar{\varphi}$ varies in $[0, \pi]$ and they represent motor cortical cell's PDs.
Therefore we submit a principal fiber bundle (E, M, F, π) as a M1 structure, where:

- $M = S^1 \times [0, \pi]$ represents arm position in the body transverse plane;
- $F = S^1 \times [0, \pi]$ represents all possible movement directions $\left(\vartheta - \bar{\vartheta}, \varphi - \bar{\varphi}\right)$ measured by the cell at position $(\vartheta, \varphi) \in M$;
- $E = M \times \left(S^1 \times [0, \pi]\right)$ represents the (arm area of the) motor cortex;
- $\pi : M \times \left(S^1 \times [0, \pi]\right) \to M$ is a surjective differential map, which locally acts as follows: $\pi\left(\vartheta, \varphi; \vartheta - \bar{\vartheta}, \varphi - \bar{\varphi}\right) = (\vartheta, \varphi)$;
- $s : M \to M \times \left(S^1 \times [0, \pi]\right)$ represents the selection of a point on a fiber of possible movement directions in response to the impulse derived from $(\vartheta, \varphi) \in M$.

Remark 4.4. Note that the parameter describing the motion of the elbow only belongs to $[0, \pi]$ (with no identification of extrema), due to physiological constraints. Also note that we are interesteed in this chapter to the local behaviour of the structure, so that we will not give a precise description of the set of parameters.

Let's resume what we have represented in describing the principal fiber bundle (E, M, F, π) as a M1 structure:

- If $q \in M$, a basis for $T_q M$ is $(\partial_\vartheta, \partial_\varphi)$;
- q expressed in joint angle coordinates is represented by (ϑ_q, φ_q);
- The fiber F over the point q has a basis given by $(\partial_\vartheta, \partial_\varphi)$.

We would like to remark that the choice of coordinates just provided can be interpreted as exponential coordinates around the point (ϑ, φ) in the fiber bundle defined above.
Indeed we can fix $(\partial_\vartheta, \partial_\varphi)$ as basis of $T_q M$ at every point, represent q in joint angle coordinates (θ_q, φ_q) and compute the canonical coordinates of the point $\left(\bar{\vartheta}, \bar{\varphi}\right)$ around the point q. According to formula (1.16) these can be computed as

$$\left(\bar{\vartheta}, \bar{\varphi}\right) = \exp\left(e_1 \partial_\vartheta + e_2 \partial_\varphi\right)(\vartheta_q, \varphi_q).$$

Consequently we get

$$e_1 = \bar{\vartheta} - \vartheta_q, \quad e_2 = \bar{\varphi} - \varphi_q.$$

Indeed,

$$\begin{cases} \gamma'(s) = \begin{pmatrix} \gamma_1'(s) \\ \gamma_2'(s) \end{pmatrix} = e_1 \begin{pmatrix} 1 \\ 0 \end{pmatrix} + e_2 \begin{pmatrix} 0 \\ 1 \end{pmatrix} \\ \\ \gamma(0) = \begin{pmatrix} \gamma_1(0) \\ \gamma_2(0) \end{pmatrix} = \begin{pmatrix} \vartheta_q \\ \varphi_q \end{pmatrix}, \end{cases}$$

therefore

$$\begin{cases} \gamma_1(s) = e_1 s + \vartheta_q \\ \gamma_2(s) = e_2 s + \varphi_q, \end{cases}$$

and since $\gamma(1) = \left(\bar{\vartheta}, \bar{\varphi}\right)$, then

$$\begin{cases} \gamma_1(1) = e_1 + \vartheta_q = \bar{\vartheta} \\ \gamma_2(1) = e_2 + \varphi_q = \bar{\varphi}, \end{cases}$$

and we get

$$\begin{cases} e_1 = \bar{\vartheta} - \vartheta_q \\ e_2 = \bar{\varphi} - \varphi_q. \end{cases}$$

Remark 4.5. Note that a choice of two angles for the shoulder joint (as exposed in subsection 4.2.2 in the paragraph dedicated to 3D movements) can shape a principal fiber bundle as a M1 structure for 3D arm movements as follows.
We can consider the quadruple (E, M, F, π), where:

- $M = S^2 \times [0, \pi]$ represents arm position in the body transverse plane;
- $F = S^2 \times [0, \pi]$ represents all possible movement directions $\left(\vartheta - \bar{\vartheta}, \varphi - \bar{\varphi}\right)$ measured by the cell at position $(\vartheta, \varphi) \in M$;
- $E = M \times \left(S^2 \times [0, \pi]\right)$ represents the (arm area of the) motor cortex;
- $\pi : M \times \left(S^2 \times [0, \pi]\right) \to M$ is a surjective differential map, which locally acts as follows: $\pi\left(\vartheta_1, \vartheta_2, \varphi; \vartheta_1 - \bar{\vartheta}_1, \vartheta_2 - \bar{\vartheta}_2, \varphi - \bar{\varphi}\right) = (\vartheta_1, \vartheta_2, \varphi)$;
- $s : M \to M \times \left(S^2 \times [0, \pi]\right)$ represents the selection of a point on a fiber of possible movement directions in response to the impulse derived from $(\vartheta_1, \vartheta_2, \varphi) \in M$.

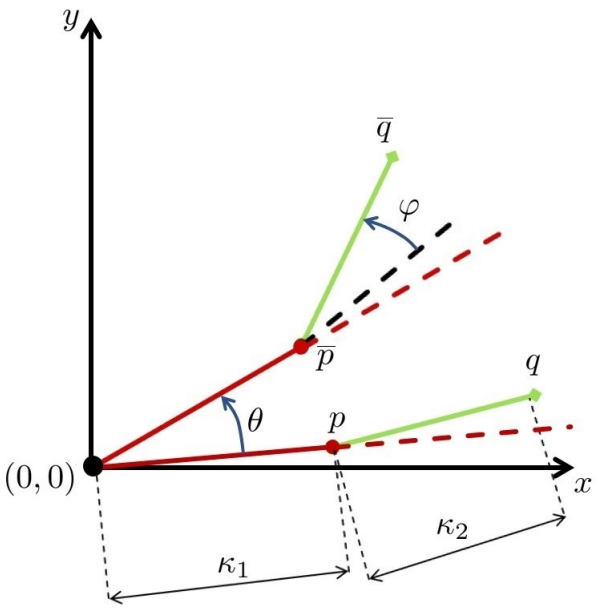

Figure 4.5: Right arm arrangement in 2D space.

The group law in the fiber

We said the previous structure is a principal fiber bundle, and we prove here which is the group law in the fiber F.

Let's call ϑ and φ respectively the shoulder and elbow rotation angle. Since we have proved that the natural internal coordinates are the exponential coordinates, not the external ones, we will measure coordinates in the fiber using the position of the arm measured in angles as origin of the fiber. We will always call (ϑ, φ) and $\bar{\vartheta}, \bar{\varphi}$ the coordinates in the fiber, using this simplified angular notation to describe the group law in the fiber. Let's consider a reference system in which the origin coincides with the shoulder joint, as shown in Figure 4.5. Let be p and q respectively the elbow and the hand position in the 2D space. We can think that point q reaches a new configuration in point $\bar{q}$ following:

1. a rotation around the origin of an angle ϑ;
2. a rotation around the point $\bar{p}$ of an angle φ, where $\bar{p}$ is obtained by a rotation around the origin of an angle ϑ applied to the point p.

In this way, denoting with $R(\cdot)$ a rotation of an arbitrary angle around the origin, we get that:

$$\bar{q} = R(\varphi)\left(R(\vartheta)\, q - R(\vartheta)\, p\right) + R(\vartheta)\, p,$$
$$\bar{p} = R(\vartheta)\, p.$$

So we ask if, once the points p and q are fixed, the set

$$\{R(\varphi)(R(\vartheta)q - R(\vartheta)p) + R(\vartheta)p, \ \ (\vartheta,\varphi) \in S^1 \times S^1\} \tag{4.1}$$

is a group.

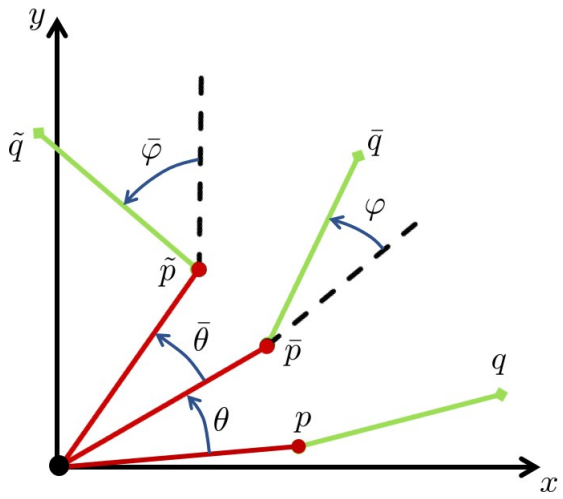

Figure 4.6: Schematic representation of the movements of the right arm in the plan to describe the group law.

A generic element of (4.1) is of the form

$$A_{\vartheta,\varphi}(p,q) = R(\varphi)(R(\vartheta)q - R(\vartheta)p) + R(\vartheta)p.$$

The set of parameters (ϑ,φ) form a group with the operation induced by the composition $A_{\vartheta,\varphi} \circ A_{\bar{\vartheta},\bar{\varphi}}$, indeed we have (following the diagram shown in Figure 4.6):

$$\begin{aligned}\bar{q} &= R(\varphi)(R(\vartheta)q - R(\vartheta)p) + R(\vartheta)p,\\ \bar{p} &= R(\vartheta)p\end{aligned}$$

and

$$\begin{aligned}\tilde{q} &= R(\bar{\varphi})\left(R\left(\bar{\vartheta}\right)\bar{q} - R\left(\bar{\vartheta}\right)\bar{p}\right) + R\left(\bar{\vartheta}\right)\bar{p},\\ \tilde{p} &= R\left(\bar{\vartheta}\right)\bar{p}.\end{aligned}$$

We point out that $\bar{\vartheta}$ and $\bar{\varphi}$ are not refer to motor cortical cell's PDs, they have the same meaning of ϑ and φ exposed at the beginning of the section dedicated to the group law.

Then

$$\begin{aligned}
\tilde{q} &= R(\bar{\varphi})\left(R\left(\bar{\vartheta}\right)(\bar{q}-\bar{p})\right)+R\left(\bar{\vartheta}\right)\bar{p}= \\
&= R(\bar{\varphi})\left(R\left(\bar{\vartheta}\right)R(\varphi)\left(R(\vartheta)\,q-R(\vartheta)\,p\right)\right)+R\left(\bar{\vartheta}\right)\bar{p}= \\
&= R(\bar{\varphi})\,R\left(\bar{\vartheta}\right)R(\varphi)\,R(\vartheta)\,q-R(\bar{\varphi})\,R\left(\bar{\vartheta}\right)R(\varphi)\,R(\vartheta)\,p+R\left(\bar{\vartheta}\right)R(\vartheta)\,p= \\
&= R(\bar{\varphi})\,R(\varphi)\left(R\left(\bar{\vartheta}\right)R(\vartheta)\,q-R\left(\bar{\vartheta}\right)R(\vartheta)\,p\right)+R\left(\bar{\vartheta}\right)R(\vartheta)\,p= \\
&= R(\bar{\varphi}+\varphi)\left(R\left(\bar{\vartheta}+\vartheta\right)q-R\left(\bar{\vartheta}+\vartheta\right)p\right)+R\left(\bar{\vartheta}+\vartheta\right)p.
\end{aligned}$$

In this way

$$A_{\vartheta,\varphi}(p,q)\circ A_{\bar{\vartheta},\bar{\varphi}}(\bar{p},\bar{q})=A_{\tilde{\vartheta},\tilde{\varphi}}(\tilde{p},\tilde{q})=A_{\vartheta+\bar{\vartheta},\varphi+\bar{\varphi}}(p,q)\,.$$

Being induced by the composition law, one can easily check that the operation in the set of parameters (ϑ,φ) verifies the group operation axioms, where the inverse of a point (ϑ,φ) is induced by $A^{-1}_{(\vartheta,\varphi)}$ and the identity element is given by the trivial point $e=(0,0)$.

Conclusions

The aim of this thesis is to develop a mathematical model of the arm area of the motor cortex. Differential models of sensory areas have been developed since '70 and the development continues up to now, thanks new data acquired with new instruments of medical images and fMRI. In particular the visual cortex has been described by Petitot and Tondut in [23] and by Citti and Sarti in [6] as a fiber bundle or a Lie group with a sub-Riemannian metric. The state of the research is completely different for the motor cortex. Data are available, but there are no models in literature, expressed in terms of differential instruments.

Hence we started the work with selecting papers describing the functional architecture of the visual cortex which could be mathematized. In particular we focused on papers of Georgopoulos, which observe the strong selectivity of movement direction of motor cortical cells [9]. In particular each cells presents a preferred movement direction. He also proved the existence of hypercolumn of direction, which we describe here as a principal fiber bundle [10]. Other papers [5] focused on the position dependency, postulating that the preferred movement direction of cells changes while changing the starting position of the arm movement.

Our main contribution has been to link this problem with the problem of finding an internal coordinates system which had already studied in [2]. In this way we were able to show that the preferred movement direction of the cell is invariant with respect to arm movement if expressed in exponential coordinates around the angle describing the initial arm position. The notion of intrinsic coordinates could be extended to more general set of movements, not limited to arm movement, but allowing for movements of the shoulders or the whole body. The resulting structures are expected to be strongly non commutative, but our theoretical framework could be naturally extended to consider this case.

An other interesting aspect is the problem of spacial organization of the motor cortical cells. From the experiments of Georgopoulos it is known that they are organized in 2D feature maps, with an approximate periodicity. The analogous structures for vision has been analyzed with different instruments, which could be extended to our setting. One of the main difficulty in the extension is the fact that some of the models are based on the exis-

tence of cells receptive fields. These models cannot adapted directly since the receptive fields in the sensory cortex take input in the visual or tactile stimulus, while the input of the motor cortex is from higher area of the cortex.

A last aspect which we think could be described with geometrical or analytic instruments is the pattern of cortical connectivity between motor cortical cells, which in a paper of Georgopoulos [11] is identified with the neural population coding.

To conclude we think that there should be a geometrical relation between the the structure of the set of selected feature (which in the present setting is position and direction of movement), their spatial organization (expressed as a fiber bundle or a pinwheel map), and their functionality (expressed in terms of connectivity).

Bibliography

[1] R. Ajemian, D. Bullock, S. Grossberg, *A model of Movement Coordinates in the Motor Cortex: Posture-dependent Changes in the Gain and Direction of Single Cell Tuning Curves.* "Cerebral Cortex", 11: 1124-1135, Dec 2001.

[2] R. Ajemian, D. Bullock, S. Grossberg, *Kinematic Coordinates In Which Motor Cortical Cells Encode Movement Direction.* J Neurophysiol 84:2191-2203, 2000.

[3] D. Barbieri, G. Citti, G. Cocci, A. Sarti, *A cortical-inspired geometry for contour perception and motion integration.* Journal of Mathematical Imaging and Vision, 2013.

[4] W. Bosking, Y. Zhang, B. Schofield, and D. Fitzpatrick, *Orientation Selectivity and the Arrangement of Horizontal Connections in Tree Shrew Striate Cortex.* J. Neurosci., 17(6):2112-2127, 1997.

[5] R. Caminiti, P.B. Johnson, A. Urbano, *Making Arm Movements Within Different Parts of Space: Dynamic Aspects in the Primate Motor Cortex.* The Journal of Neuroscience, July 1990, 10(7): 2039-2058.

[6] G. Citti, A. Sarti, *Models of the Visual Cortex in Lie Groups.* Advanced Courses in Mathematics, Springer, 2013.

[7] D. Field, A. Hayes, and R. Hess, *Contour integration by the human visual system: Evidence for a local association field.* Vision Research, 33(2):173-193, January 1993.

[8] T. Frankel, *The geometry of physics: an introduction.* Cambridge University Press, 2011.

[9] A.P. Georgopoulos, *Columnar Organization of the Motor Cortex: Direction of Movement.* Springer Science+Business Media Dordrecht 2015. M.F. Casanova, I. Opris (eds.), "Recent Advances on the Modular Organization of the Cortex", DOI 10.1007/978-94-017-9900-38.

[10] A.P. Georgopoulos, H. Merchant, T. Naselaris, B. Amirikian, *Mapping of the preferred direction in the motor cortex*. PNAS, vol. 104, June 2007, 11068–11072.

[11] A. P. Georgopouls, A.B. Schwartz, R. E. Ketiner, *Neuronal Population Coding of Movement Direction*. Downloaded from www.sciencemag.org on December 26, 2006.

[12] A. P. Georgopouls, J. F. Kalaska, R. Caminiti, J. T. Massey, *On the relations between the direction of two-dimensional arm movements and cell discharge in primate motor cortex*. The Journal of Neuroscience, Vol. 2, No. 11, pp. 1527-1537, November 1982.

[13] A. P. Georgopoulos, R. E. Kettner, B. Scwartz, *Primate Motor Cortex and Free Arm Movements to Visual Trgets in Three-Dimensional Space. II. Coding of Movement by a Neuronal Population*. The Journal of Neuroscience, August 1988, 8(8):2928-2937.

[14] A. P. Georgopoulos, *Spatial coding of visually guided arm movements in primary motor cortex*. J. Physiol. Pharmacol. 66: 518-526, 1988.

[15] S. Hocherman, S.P. Wise, *Effects of hand movement path on motor cortical activity in awake, behaving rhesus monkeys*. Experimental Brain Research, (1991) 83:285-302.

[16] W. Hoffman, *Higher visual perception as prolongation of the basic lie transformation group*. Mathematical Biosciences, 6:437-471, 1970.

[17] D. Hubel, *Eye, Brain, and Vision (Scientific American Library, No 22)*. W. H. Freeman, 2nd edition, May 1995.

[18] D. Hubel and T. Wiesel, Ferrier lecture: *Functional architecture of macaque monkey visual cortex*. Royal Society of London Proceedings Series B, 198:1-59, May 1977.

[19] J. Jost, *Riemannian Geometry and Geometric Analysis*, Springer- Verlag Berlin Heidelberg, 2011.

[20] E. Le Donne, *Lecture notes on sub-Riemannian geometry*. http://enrico.ledonne.googlepages.com/, version of Summer 2017

[21] V.B. Mountcastle (1997), *The columnar organization of the neocortex*. Brain 120:701–722

[22] J. Petitot, *Neurogeometrie de la Vision Modeles, Mathematiques et Physiques des Architectures Fonctionnelles*. Ecole Polytechnique, 2008.

[23] Petitot, J., Tondut, Y., *Vers une Neurogéométrie. Fibrations corticales, structures de contact et contours subjectifs modaux*. Mathematiques, Informatique et Sciences Humaines, 1999, 145, EHESS, CAMS, Paris, pp. 5-101.

[24] G. Sanguinetti, *Invariant models of vision between phenomenology, image statistics and neurosciences*. PhD thesis, Universidad de la República, Montevideo, Uruguay, 2011. Director-Gregory Randall.

[25] A. Sarti, G. Citti, J. Petitot, *Functional Geometry of the Horizontal Connectivity in the Primary Visual Cortex*, "Journal of physiology", 2009,103, pp. 37-45.

[26] A. Sarti, G. Citti, and J. Petitot, *The symplectic structure of the primary visual cortex*. "Biological Cybernetics", 98(1):33-48, 2008.

[27] A. B. Schwartz, R.E. Kettner, A.P. Georgopoulos, *Primate Motor Cortex and Free Arm Movements to Visual Targets in Three-Dimensional Space. I. Relations Between Single Cell Discharge and Direction of Movement*. The Journal of Neuroscience, August 1988, 8(8): 2913-2927.

[28] J. Selig, *Introductory robotics*. Vol 5, Prentice Hall London, 1992.

[29] W. W. Teka, K. C. Hamade, W. H. Barnett, T. Kim, S. N. Markin, I. A. Rybak, Y. I. Molkov, *From the motor cortex to the movement and back again*. PLoS ONE 12(6): e0179288, June 2017.

Ringraziamenti

Grazie mille alla Professoressa Citti, per la sua premura e per avermi insegnato la matematica più bella che io abbia mai conosciuto. Grazie infinite anche ad Emre, per il suo talento e generosità. Grazie alle professoresse Piumi e Di Pietro, per la passione con cui avete insegnato.
Grazie mama e babo. Grazie Michele, per la tua arguta schiettezza. Grazie Giulio per il tuo cuore d'oro. Grazie Chemy, per il tuo entusiasmo. Grazie Giuly, perché con te è sempre casa. Grazie Freccia, per tutti i pensieri e il tuo coraggio. Grazie Fede, per la cura che hai. Grazie Ilarià, perché già hai capito. Grazie Ingrid, perché con te non è mai ciò che sembra. Grazie Chiara, perché conosci il prossimo. Grazie Deb, perché vivi nel mio cuore. Grazie Rinno, perché l'insicurezza ti rende grande. Grazie Chiara, perché sei la verità. Grazie Mary, per la tua tenacia. Grazie Marco, per la tua resilienza. Grazie mille Clo, Polli, Sere, Kerol, Fede, Lory, perché una squadra è una famiglia.
Grazie a tutti di cuore.